# Vinculin targeting by *Shigella* IpaA promotes stable cell adhesion independent of mechanotransduction

Cesar Valencia-Gallardo[1-4]*, Daniel-Isui Aguilar-Salvador[1-4]*, Hamed Khakzad[5, 7§], Charles Bou-Nader[8, 9§], Christian Malosse[10], Diogo Borges Lima[10], Chakir Bello[1-4], Benjamin Cocom-Chan[1-4], Nicole Quenech'Du[1-4], Bilal Mazhar[1-4], Delphine Javelaud[11-13], Jacques Fattaccioli[14, 15], Alain Mauviel[11-13], Marc Fontecave[8, 9], Atef Asnacios[16], Julia Chamot-Rooke[10], Lars Malmström[5, 7, 17], Guy Tran Van Nhieu[1-4¶*]

[1]Equipe Communication Intercellulaire et Infections Microbiennes, Centre de Recherche Interdisciplinaire en Biologie (CIRB), Collège de France, 75005 Paris, France

[2]Institut National de la Santé et de la Recherche Médicale U1050, 75005 Paris, France

[3]Centre National de la Recherche Scientifique UMR7241, 75005 Paris, France

[4]MEMOLIFE Laboratory of excellence and Paris Science Lettre

[5]Institute for Computational Science, University of Zürich, Zürich, Switzerland.

[6]S3IT, University of Zürich, Zürich, Switzerland.

[7]Swiss Institute of Bioinformatics, Lausanne, Switzerland.

[8]Laboratoire de Chimie des Processus Biologiques, Collège De France, 75005 Paris, France.

[9]Centre National de la Recherche Scientifique UMR8229, 75005 Paris, France

[10] Mass Spectrometry for Biology Utechs, Institut Pasteur, USR 2000, CNRS, 75015 Paris, France

[11]Institut Curie, PSL Research University, INSERM U1021, CNRS UMR3347, Team "TGF-ß and Oncogenesis", Equipe Labellisée LIGUE 2016, F-91400, Orsay, France.

[12]Université Paris-Sud, F-91400, Orsay, France.

[13]Centre National de la Recherche Scientifique UMR 3347, 91400 Orsay, France

[14]PASTEUR, Département de Chimie, École Normale Supérieure, PSL University, Sorbonne Université, CNRS, 75005 Paris, France

[15]Institut Pierre-Gilles de Gennes pour la Microfluidique, 75005 Paris, France

[16]Laboratoire Matière et Systèmes Complexes, UMR 7057 CNRS & Université Paris Diderot, Sorbonne Paris Cité, Paris, France

[17]Division of Infection Medicine, Department of Clinical Sciences, Lund University, Lund, Sweden.

*, §equal contribution

¶For correspondence:

E-mail: guy.tran-van-nhieu@college-de-france.fr. Tel: 33-1-44-27-14-89. FAX: 33-1-44-27-14-19

***Shigella*, the causative agent of bacillary dysentery, invades epithelial cells by injecting type III effectors that locally reorganize the actin cytoskeleton[1]. The type III effector IpaA targets the focal adhesion protein vinculin to induce bacterial adhesion associated with the recruitment of mature focal adhesion markers, despite the inability of bacteria to exert significant counter-forces[2, 3]. Here, we show that three vinculin-binding sites (VBSs) exposed at the IpaA C-terminus act in a cooperative manner to trigger a yet unreported mode of vinculin activation through specific interactions with sites in the vinculin head sub-domain D2. Structural modeling based on the mass spectrometry identification of interacting residues by cross-linking indicated that upon IpaA binding to vinculin D2, vinculin head sub-domains undergo major conformational changes leading to higher order heterocomplexes and vinculin homo-trimers. IpaA-mediated vinculin activation induces the formation of large and stable focal adhesions resisting the action of actin relaxing drugs. This property enables IpaA to rapidly elicit strong cell adhesion to fibronectin-coated substrates. While *Shigella* IpaA promotes strong adhesion in the absence of mechanotransduction,**

**its mode of vinculin activation likely reflects a key step during maturation of cell adhesions driven by acto-myosin contractility.**

Integrin-mediated cell adhesion critically depends on the cytoskeletal linkers talin and vinculin[4-6]. During mechanotransduction, talin acts as a mechanosensor by exposing its VBSs as a function of the stretching force generated by acto-myosin and dependent on substrate stiffness[7]. Talin exposed VBSs recruit and activate vinculin, reinforcing anchorage to the actin cytoskeleton in response to mechanical load[8, 9]. Vinculin contains three repetitions (D1-D3) of a conserved domain consisting of two bundles of four helices, and a fourth D4 domain containing only one helical bundle connected to a proline-rich unstructured region and the carboxyterminal F-actin binding domain[10]. Under its inactive folded form, intramolecular interactions between the vinculin head and tail domains prevent ligand binding.

The *Shigella* type III invasion effector IpaA contains 3 VBSs located in its carboxyterminal moiety[11-13]. IpaA VBS1, as for all VBSs described to date to promote vinculin activation, interacts with the first helical bundle of the D1 domain, promoting major conformational changes that disrupt the D1-tail intramolecular interactions and free the vinculin F-actin binding region[11] (Fig. 1a). IpaA VBS2, in contrast, interacts with the second helical bundle of D1[12] (Fig. 1a) and its association with IpaA VBS1 results in a very high affinity and stable IpaA VBS1-2:D1 complex ,with an estimated $K_D$ in the femtoM range[12]. While functional evidence indicates that IpaA VBS3 cooperates with IpaA VBS1-2 to stimulate bacterial invasion, the isolated peptide acts as IpaA VBS1 in promoting vinculin activation through interaction with the vinculin D1 first helical bundle and also forms a folded bundle with the talin H1-H4 helices[13, 14].

Here, we studied the effects of the IpaA subdomains containing VBS1-2 (A524) or VBS1-3 (A483) on vinculin activation (Fig. 1b). We performed SEC-MALS (Size Exclusion Chromatography-Multi-Angle Light Scattering) to analyze complexes formed upon incubation of A483 with $HV_{1-834}$ containing the D1-D4 domains, corresponding to full-length human vinculin (HV) devoid of the

carboxyterminal F-actin binding domain (Fig. 1b). In addition to the 1:1 D1D4: A483 complex, larger complexes were observed corresponding to a 2:1 heterocomplex and a 3:0 D1-D4 homo-trimer (Fig. 1c). Similar 2:1 and 3:0 complexes were observed when A483 was incubated with $HV_{1-484}$ containing only the vinculin D1 and D2 domains (D1D2) (Fig. 1d), indicating that vinculin homo-trimerization occurs exclusively through these vinculin head sub-domains. By contrast, when A524 was incubated with D1D2, 1:1 and 2:1 D1D2:A524 complexes were detected, but not the D1D2 homo-trimer suggesting a role for IpaA VBS3 in vinculin trimerization (Fig. 1d). Consistently, higher order D1D2 homo-complexes devoid of A483 and D1D2:A524 hetero-complexes were visualized by native PAGE (Fig. 1e and Suppl. Figs. 3c, d). These results suggest that binding of IpaA VBSs to vinculin triggers conformational changes in vinculin leading to the formation of an IpaA VBS3-dependent vinculin homo-trimer.

To further investigate initial interactions responsible for vinculin trimer formation, w e performed binding assays with HV derivatives immobilized onto a solid phase to restrict conformational changes. These assays indicated that A483 and A524 bound to HV with a similar affinity, as estimated by their EC50 (95% confidence interval) of 6.1 (4.2-9.0) and 3.7 (1.7-8.1) nM, respectively (Suppl. Fig. 1a). Strikingly, a large difference was observed in the binding plateau, indicating that HV presented more binding sites for A483 than for A524 (Suppl. Fig. 1a). Also, D1D2 presented more binding sites for $HV_{1-258}$ containing the D1 domain only, suggesting the presence of additional sites on the D2 domain (Suppl. Fig. 1b). Consistently, BN-PAGE showed the formation of 1:1, as well as a 1:2 D1D2:A483 complex, observed with increasing A483 molar ratio (Suppl. Fig. 1c). In contrast, single 1:1 complexes were observed for D1:A483, D1:A524 or D1D2-A524 (Suppl. Figs. 1c-h), indicating that IpaA VBS3 was required to reveal additional sites on the D2 domain. Of note, D1D2 homo-trimers observed in the SEC-MALS and native gel analysis (Figs. 1d, e and Ext Data Figs. 3c, d) were not detected in BN-PAGE, suggesting that Coomassie brilliant blue interfered with the formation of higher order D1D2 complexes. Together, these results suggested that the formation of vinculin trimers triggered by A483 required the IpaA VBS3 dependent exposure of binding sites on D2. These findings were

unexpected, since vinculin activating ligands have been described to bind to a single site on the D1 domain of vinculin.

To map interactions of A524 and A483 with D1D2, complexes were cross-linked, subjected to proteolysis and analyzed using Liquid Chromatography coupled to Mass Spectrometry (LC-MS) (Methods). Intermolecular links were identified from the characterization of cross-linked peptides (Suppl. Tables 1-3; Methods) and along with identified intramolecular links, used to produce structural models (Methods). The A524:D1 complex showed links consistent with a "canonical" conformer expected from established structures[11, 12, 15] (Suppl. Fig. 2). Similar links were identified for the A524:D1D2 complex, with a majority of links observed with the D1 domain (Fig. 2a). For both complexes, the structure shows interactions between IpaA VBS1 and VBS2 with the D1 first and second bundles, respectively, leading to helical bundle reorganization of D1 associated with vinculin activation (Figs. 2c, d; Suppl. Fig. 2 and Suppl. Tables 1, 2). For the A483:D1D2 complex, structural modeling shows 2 major conformers accounting for the majority of links. In a first "closed" conformer, IpaA VBS1 and VBS2 interact with the D1 bundles in a similar manner as for A524, where the relative positioning of D1 and D2 is globally conserved compared to apo D1D2 in the A524-D1D2 complex (compare Figs. 2d and 2e). In this “closed” conformer, IpaA VBS3 interacts with an interface formed by the H5 (residues 128-149) and H8 (residues 222-250) helices in the second bundle of D1 and the H13 (residues 373-397) helix in the second bundle of the D2 domain (Figs. 2e and f). The second "open" conformer, however, shows a major re-orientation of D1 and D2 subdomains with their major axis forming an angle value of ca 82° compared to the 25° observed in the native vinculin structure or the first conformer (Fig. 2g), with IpaA VBS3 docking sidewise through extensive interaction with the H5 (residues 128-149) and H8 (residues 222-250) helices of the vinculin D1 domain. Because this latter conformer leads to major changes in bundle exposure in D1 and D2, we posit that it is involved in the formation of higher order D1D2 complexes and trimer induced by A483. To test this, we engineered a structural clamp by substituting residue Q68 in the first D1 bundle and A396 in the second D2 bundle for cysteine residues, expected to prevent the formation of the open

conformer upon disulfide bridge formation (Suppl. Figs. 3a, b). Consistently, cysteine clamped D1D2-Q68C A396C did not prevent the exposure of additional sites on D2 or 1:1 complex formation induced by A524 or A483, but prevented the formation of higher order complexes (Fig. 1 e and Suppl. Figs. 3c-e). We coined "supra-activation" the mode of vinculin activation induced by A483 involving major conformational changes in the vinculin head, to distinguish it from the canonical activation associated with the dissociation of vinculin head-tail domains.

We then characterized the effects of A524 and A483 expression by performing immunofluorescence staining of vinculin-containing adhesion structures. As shown in Figs 3a-c, C2.7 cells transfected with GFP-A524 formed more numerous and larger peripheral adhesions as well as actin-rich ruffles compared to control cells (Figs. 3a-d). Strikingly, GFP-A483 transfected cells formed even larger and more numerous adhesions than GFP-A524 transfected cells, but significantly less actin ruffles than GFP-A524 transfectants (Figs. 3a-d). These observations were confirmed by live TIRF microscopy showing the extreme stability of adhesions in GFP-A483 transfectants, with a median duration of at least 84 min, while GFP-A524 and control cells showed adhesions with a comparable median duration of less than 25 min (Fig. 3e; Suppl. movie 1). GFP-A524 and GFP-A483 transfectants showed slightly slower median instant rates of adhesion assembly than control cells (Suppl. Fig. 4; Suppl. movie 1) but significant 1.6-fold and 2-fold decrease in median instant rates of disassembly relative to control cells, respectively (Suppl. Fig. 4). The stability of GFP-A483-induced FAs was independent of acto-myosin contraction. Indeed, GFP-A483-induced FAs resisted the action of the Rho-kinase inhibitor Y27632 relaxing actin-myosin, with a five- and four-times slower median rate of disassembly of adhesions relative to control cells and GFP-A524 transfectants, respectively (Figs. 3f-i; Suppl. movie 2). Furthermore, large adhesions formed in GFP-A483 transfectants following addition of the inhibitor (Figs. 3f, h), a process that was not observed for the other samples, including cells transfected with GFP-A524 or GFP fused to the vinculin D1 domain (vD1) reported to delay talin refolding following stretching [16-18] (Figs. 3g-i; Suppl. movie 2). In line with the stabilization of mature FAs through vinculin supra-activation, GFP-A483 but not GFP-vD1 also delayed the Y27632-induced

148 removal of the late adhesion marker VASP (Suppl. Fig. 5; Suppl. movie 3). Consistent with A483
149 bypassing mechanotransduction, GFP-A483 expression induced 5- and 1.6-fold higher yield of short
150 term (≤ 10 min) cell adhesion to fibronectin substrates compared to control GFP and GFP-A524
151 transfectants, respectively (Suppl. Fig. 6a). By contrast, little difference in adhesion yield was
152 detected at 15 min suggesting that canonical activation of vinculin also resulted in its supra-activation
153 during mechanotranduction (Suppl. Fig. 6a). In line with this, MEF vinculin-null cells transfected with
154 the clamped vinculin version formed fewer and smaller FAs than cells transfected with wild-type
155 vinculin but more than mock-transfected cells (Suppl. Figs. 6b-d).

156 To confirm and extend these findings, cell adhesion strength was assessed measuring their
157 detachment upon application of a controlled shear stress in a microfluidic chamber. When 1205Lu
158 melanoma cells were allowed to adhere to fibronectin-coated surfaces for more than 25 min, little
159 difference in resistance to shear stress could be detected among samples (Suppl. Fig. 7a). In contrast,
160 when shear stress was applied less than 20 min following cell incubation, GFP-A483-transfected cells
161 showed significantly higher resistance to shear stress up to 22.2 dynes.cm$^{-2}$ than GFP-A524- or GFP-
162 transfected cells, with 1.7 ± 0.2 -and 0.9 ± 0.14-fold enrichment ± SD of adherent cells for GFP-A483
163 and GFP-A524-transfected cells versus control GFP-transfected cells, respectively (Fig. 4b; Suppl.
164 movie 4). In addition, similar to melanoma cells depleted for by siRNA treatment, cells transfected
165 with the clamped vinculin version showed a decreased ability to adhere in comparison to WT
166 vinculin-transfected cells (Suppl. Figs. 7a, b). These results are in full agreement with effects observed
167 on adhesion structures and suggest that A483 interaction with vinculin leads to the bypass of
168 mechanotransducing steps to promote strong adhesion.

169 Vinculin is paradoxically described as a prognostic marker favoring the migration of cancer cells
170 or as a tumor suppressor stimulating cell anchorage [19-21]. These contradictory findings reflect its
171 complex and poorly understood regulation, as well as different roles in 2D or 3D systems [22, 23]. Also,
172 an increase of the total pool of vinculin may not correlate with increased vinculin activation. We took
173 advantage of the unique property of A483 to study the effects of vinculin supra-activation on the

motility and invasion of melanoma cells. In time-lapse microscopy experiments in 2D-chambers, GFP-A524 inhibited melanocyte motility compared to control cells, with a rate of Root Median Square Displacement (rMSD) of 3.16 and 15.6 µm.min, respectively (Figs. 4c, d). An even stronger inhibition was observed for GFP-A483-transfected cells (rMSD = 2.3 µm.min) (Figs. 4c, d). Transmigration of melanocytes in 3D-matrigels was similarly inhibited by A524 and A483 (Fig. 4e).

Bacteria invading through a triggering mode rely on a discrete number of T3SS-dependent contacts for which cytoskeletal tethering is likely critical for invasion[2]. As opposed to physiological substrates, bacteria cannot sustain the range of counter-forces associated with integrin-mediated adhesion to the substrate. The *Shigella* type III effector IpaA provides an elegant solution to this problem by promoting strong adhesion without requirement for mechanotransduction. Through the joint action of its VBSs, IpaA induces major conformational changes of the vinculin head sub-domains. Understanding how these major vinculin conformational changes regulate the composition and properties of cell adhesions will bring important insights into cell adhesion processes and will be the focus of future investigations.

## REFERENCES

1 Ogawa, M., Handa, Y., Ashida, H., Suzuki, M. & Sasakawa, C. The versatility of *Shigella* effectors. *Nat Rev Microbiol* **6**, 11-16, doi:10.1038/nrmicro1814 (2008).

2 Valencia-Gallardo, C. M., Carayol, N. & Tran Van Nhieu, G. Cytoskeletal mechanics during *Shigella* invasion and dissemination in epithelial cells. *Cellular microbiology* **17**, 174-182, doi:10.1111/cmi.12400 (2015).

3 Tran Van Nhieu, G., Ben-Ze'ev, A. & Sansonetti, P. J. Modulation of bacterial entry into epithelial cells by association between vinculin and the *Shigella* IpaA invasin. *The EMBO journal* **16**, 2717-2729, doi:10.1093/emboj/16.10.2717 (1997).

4 Atherton, P., Stutchbury, B., Jethwa, D. & Ballestrem, C. Mechanosensitive components of integrin adhesions: Role of vinculin. *Exp Cell Res*, doi:10.1016/j.yexcr.2015.11.017 (2015).

5 Yan, J., Yao, M., Goult, B. T. & Sheetz, M. P. Talin Dependent Mechanosensitivity of Cell Focal Adhesions. *Cellular and molecular bioengineering* **8**, 151-159, doi:10.1007/s12195-014-0364-5 (2015).

6 Burridge, K. & Guilluy, C. Focal adhesions, stress fibers and mechanical tension. *Exp Cell Res*, doi:10.1016/j.yexcr.2015.10.029 (2015).

7 Parsons, J. T., Horwitz, A. R. & Schwartz, M. A. Cell adhesion: integrating cytoskeletal dynamics and cellular tension. *Nat Rev Mol Cell Biol* **11**, 633-643, doi:10.1038/nrm2957 (2010).

8 Humphries, J. D. *et al.* Vinculin controls focal adhesion formation by direct interactions with talin and actin. *J Cell Biol* **179**, 1043-1057, doi:10.1083/jcb.200703036 (2007).

9 Lavelin, I., Wolfenson, H., Patla, I., Henis, Y. I., Medalia, O., Volberg, T., Livne, A., Kam, Z., Geiger, B**.** Differential effect of actomyosin relaxation on the dynamic properties of focal adhesion proteins. PLoS One. 8:e73549 (2013).

10 Bakolitsa, C. *et al.* Structural basis for vinculin activation at sites of cell adhesion. *Nature* **430**, 583-586, doi:10.1038/nature02610 (2004).

11 Izard, T., Tran Van Nhieu, G. & Bois, P. R. Shigella applies molecular mimicry to subvert vinculin and invade host cells. *J Cell Biol* **175**, 465-475, doi:10.1083/jcb.200605091 (2006).

12 Tran Van Nhieu, G. & Izard, T. Vinculin binding in its closed conformation by a helix addition mechanism. *The EMBO journal* **26**, 4588-4596, doi:10.1038/sj.emboj.7601863 (2007).

13 Park, H., Valencia-Gallardo, C., Sharff, A., Tran Van Nhieu, G. & Izard, T. Novel vinculin binding site of the IpaA invasin of *Shigella*. *J Biol Chem* **286**, 23214-23221, doi:10.1074/jbc.M110.184283 (2011).

14 Valencia-Gallardo C, Bou-Nader C, Aguilar D, Carayol N, Quenech'Du N, Pecqueur L, Park HJ, Fontecave M, Izard T, Tran Van Nhieu G. *Shigella* IpaA binding to talin stimulates filopodial capture and cell adhesion. *Cell Reports* **26**, 921-932. doi: 10.1016/j.celrep.2018.12.091 (2019).

15 Izard, T. *et al.* Vinculin activation by talin through helical bundle conversion. *Nature* **427**, 171-175, doi:10.1038/nature02281 (2004).

16 del Rio, A. *et al.* Stretching single talin rod molecules activates vinculin binding. *Science* **323**, 638-641, doi:10.1126/science.1162912 (2009).

17 Margadant, F. *et al.* Mechanotransduction in vivo by repeated talin stretch-relaxation events depends upon vinculin. *PLoS Biol* **9**, e1001223, doi:10.1371/journal.pbio.1001223 (2011).

18 Carisey, A. *et al.* Vinculin regulates the recruitment and release of core focal adhesion proteins in a force-dependent manner. *Curr Biol* **23**, 271-281, doi:10.1016/j.cub.2013.01.009 (2013).

19 Goldmann, W. H. Role of vinculin in cellular mechanotransduction. *Cell Biol Int* **40**, 241-256, doi:10.1002/cbin.10563 (2016).

20 Labernadie, A. *et al.* A mechanically active heterotypic E-cadherin/N-cadherin adhesion enables fibroblasts to drive cancer cell invasion. *Nat Cell Biol* **19**, 224-237, doi:10.1038/ncb3478 (2017).

21 Hamidi, H. & Ivaska, J. Every step of the way: integrins in cancer progression and metastasis. *Nat Rev Cancer*, doi:10.1038/s41568-018-0038-z (2018).

22 Mierke, C. T. *et al.* Vinculin facilitates cell invasion into three-dimensional collagen matrices. *J Biol Chem* **285**, 13121-13130, doi:10.1074/jbc.M109.087171 (2010).

23 Gulvady, A. C., Dubois, F., Deakin, N. O., Goreczny, G. J. & Turner, C. E. Hic-5 expression is a major indicator of cancer cell morphology, migration, and plasticity in three-dimensional matrices. *Mol Biol Cell* **29**, 1704-1717, doi:10.1091/mbc.E18-02-0092 (2018).

## ACKNOWLEDGEMENTS

The authors thank Gauthier Mercante for technical help, Philippe Mailly for help with image analysis and René-Marc Mège for insightful discussions and reading of the manuscript. This work was supported by grants from Inserm, CNRS and Collège de France to the CIRB, as well as grant from the PSL Idex project “Shigaforce”. DIAS and BCC are recipients of a PhD fellowship from a CONACYT scholarship. CV-G and DIAS also received support from the Memolife Labex. HK and LM were supported by Swiss National Science Foundation (grant no. SNF 200021 160188) and LM by the Knut And Alice Wallenberg Foundation (grant no. KAW 2016.0023).

## AUTHOR CONTRIBUTIONS

CV-G and DIAS conceived and performed most of the experimental works, data analysis and wrote the manuscript. BCC and BM analyzed TIRF experiments. CB-N performed the SEC-MALS analysis. CB and NQD performed and analyzed experiments with melanocytes with the help of DJ and AM. BCC, AA and JF provided technical help for cell adhesion and microfluidics experiments. CM and JCR designed and performed the LC-MS analysis. DBL analyzed the cross-linked mass spectrometry data. HK and LM generated structural models. GTVN designed the project and wrote the manuscript.

## FIGURES AND LEGENDS

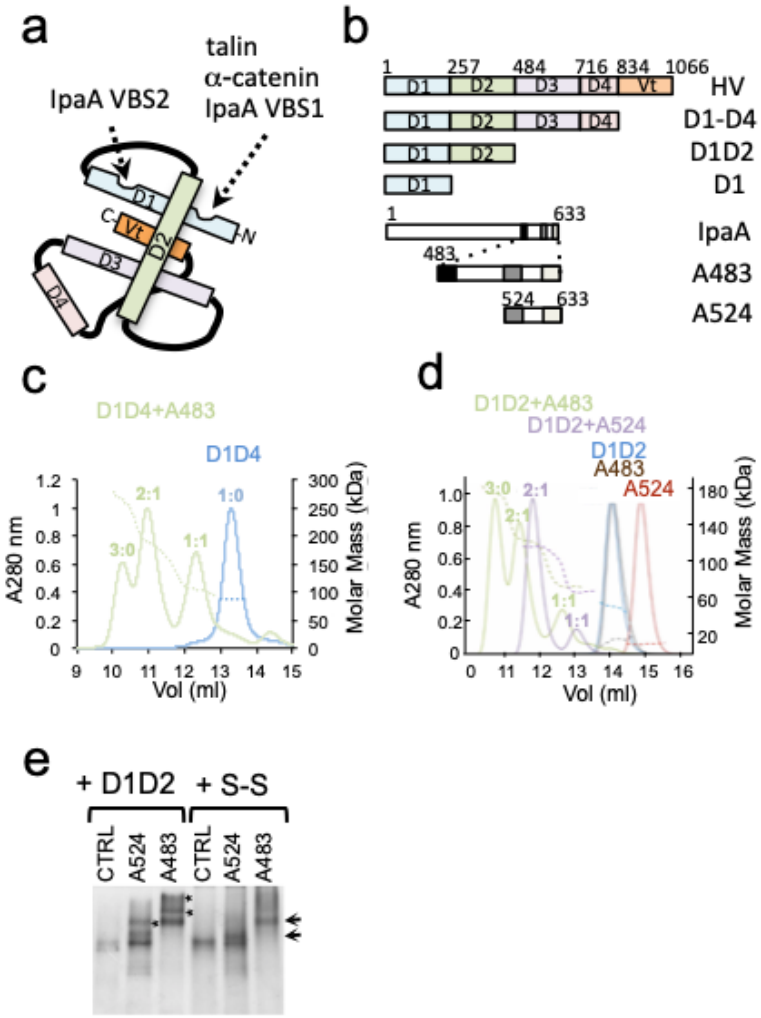


**Figure 1 – IpaA reveals binding sites in vinculin head subdomains**

**a,** Scheme of folded vinculin (HV). The binding sites and corresponding ligands are indicated. **b,** Scheme of HV and IpaA constructs. HV domains and IpaA VBSs are depicted as boxes. The numbers indicate the start residue of each domain. **c, d,** SEC elution profiles of complexes formed between A483 (green) or A524 (purple) and vinculin D1D4 (**c**) or D1D2 (**d**). The indicated complex stoichiometry was inferred from the molecular weight estimated by MALS. **e**, native gel analysis of vinculin D1D2 and IpaA derivatives. D1D2 or cysteine-clamped D1D2 (S-S) were incubated with the indicated IpaA derivatives and analyzed by native PAGE followed by Coomassie staining. Arrows: 1:1 complexes. *: higher order complexes. Note the absence of higher order complexes for cysteine-clamped D1D2.

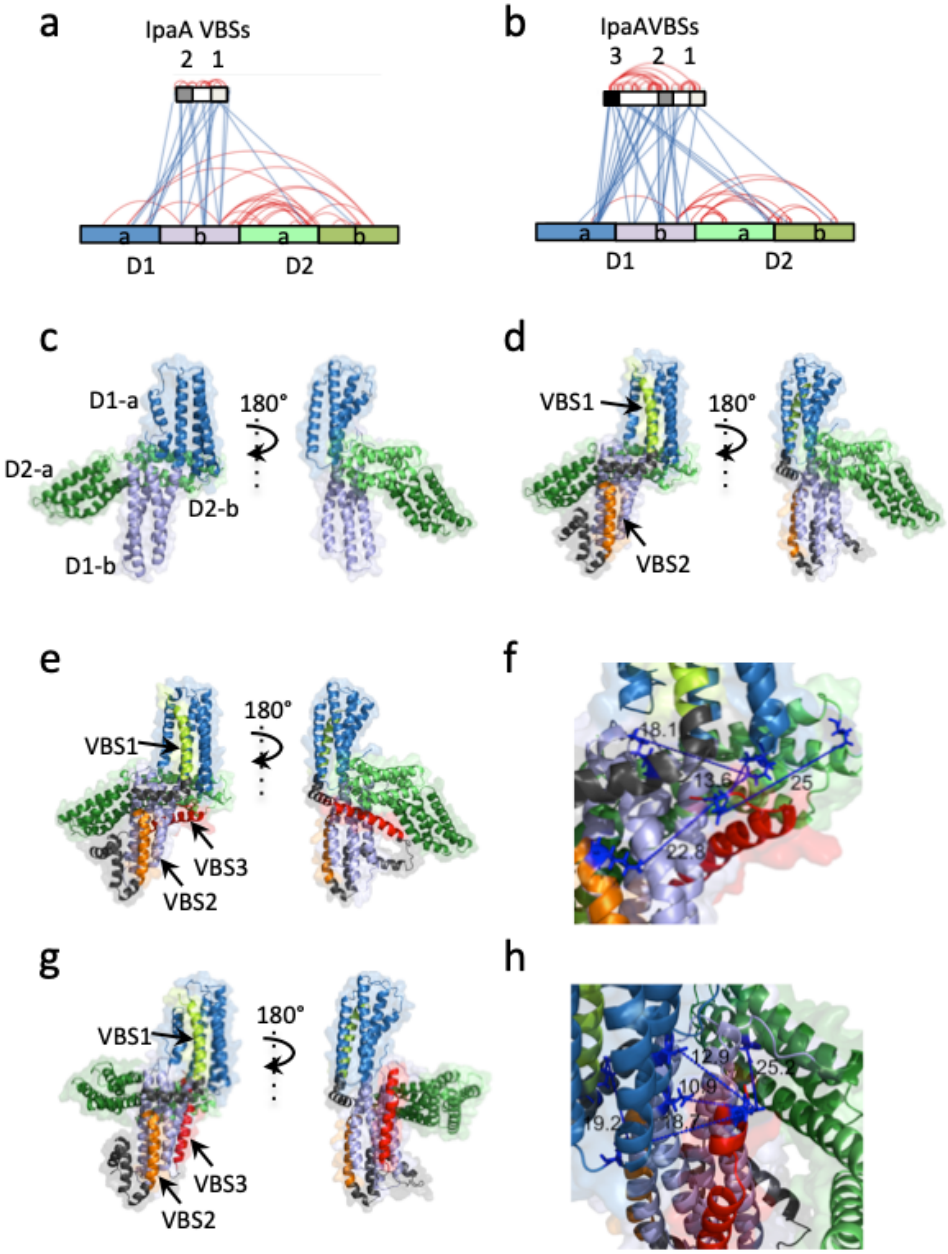


**Figure 2 – Characterization of IpaA contact sites on vinculin.**

**a**, **b**, EDC cross-link map from mass spectrometry analysis (LC-MS/MS) of vinculin D1D2-A524 (**a**) and D1D2-A483 (**b**) following extraction of 1:1 complexes from BN-PAGE. Blue lines: inter-molecular links. Red lines: intra-molecular links. Note the links between IpaA VBS3 and the D2 second bundle. Cross-linked residues are detailed in Suppl. Table 1. **c-e**) Structural models of D1D2 (**c**), D1D2-A524 (**d**), D1D2-A483 "closed" conformer (**e**), D1D2-A483 "open" conformer **(g)**. **f**, **h**, higher magnification of the IpaA

VBS3-D1D2 interaction in (**e**) and (**g**) showing the distance between residues in Å. IpaA VBS1-3 were docked on the surface of Vinculin D1D2 using MS cross-link constraints. TX-MS protocol in combination with MS constraints was used to unify and adjust the final model, which justifies over 100 cross-links.

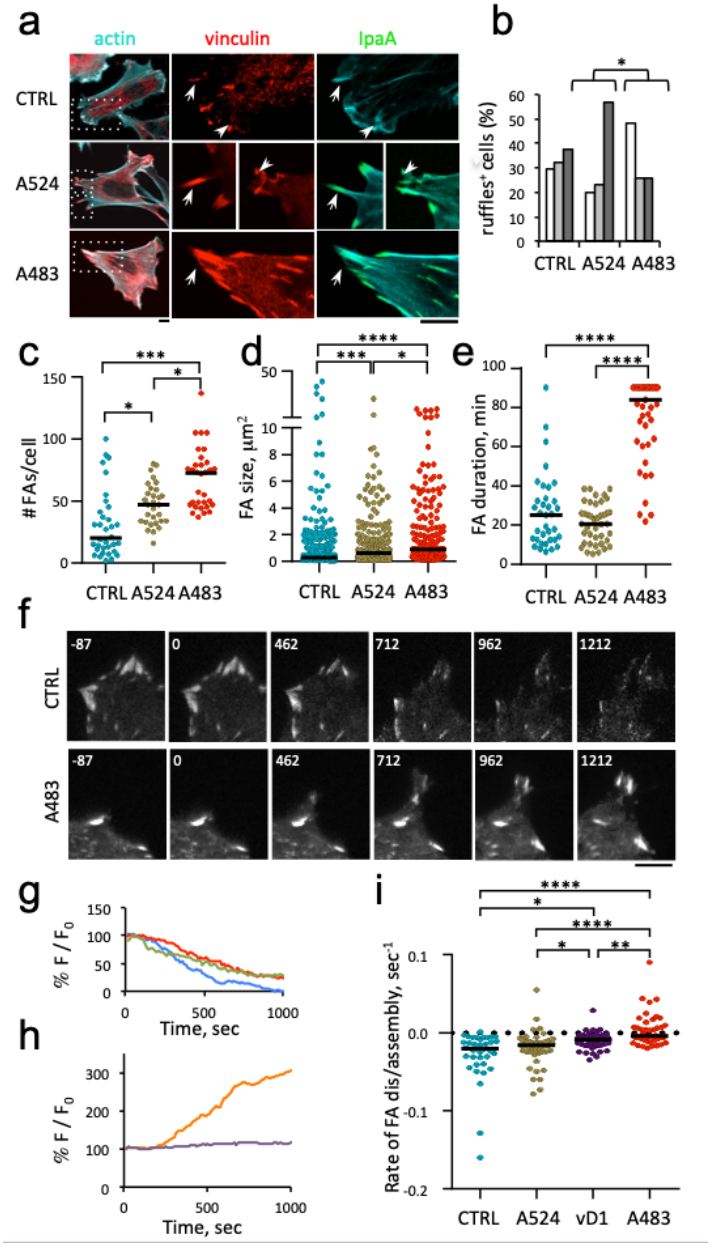


**Figure 3 – A483 stabilizes vinculin in cell adhesions in the absence of mechanotransduction**

**a-c**, Immunofluorescence analysis of vinculin adhesions. CTRL: C2.7 cells. A524: GFP-A524 transfectants. A483: GFP-A483 transfectants. **a,** representative fluorescence micrographs. Arrows: adhesions; arrowheads: ruffles. Green: GFP; red: vinculin; cyan: actin. **b**, percent of cells with ruffles ±

SEM. Cells with: no ruffles (empty bars); small ruffles (light grey bars); large ruffles (dark grey bars). *: Pearson's Chi-squared test (N=3, n > 30, p = 0.036). **c**, **d**, vinculin containing FAs were detected using a semi-automated program. **c**, median number of FAs per cell; **d**, FA size. (N=3, n > 30). Dunn's multiple comparisons test. *: $p < 0.05$;***: $p < 0.005$. **e**, TIRF microscopy of C2.7 cells transfected with mCherry-vinculin alone (CTRL) or co-transfected with GFP-A524 (A524), GFP-vD1 (vD1), or GFP-A483 (A483). The duration of vinculin-containing adhesions was determined from time-lapse acquisitions. **f-i**, TIRF microscopy analysis of cells treated with 100 µM Y-27632. **f,** Representative time series acquisitions. Numbers indicate the elapsed time in seconds, with the inhibitor added at t = 0. Scale bar = 5 µm. **g, h**, $F/F_0$: normalized average fluorescence intensity of adhesions as a function of time. Representative traces corresponding to single adhesions for: **h**, control cells: blue, A524: red, vD1: green; **g**, A483: purple and orange. **i,** initial rates of adhesion disassembly inferred from linear fits. N = 5. Number of adhesions analyzed: CTRL: 84; vD1: 75; A524: 140; A483: 97. Dunn's multiple comparisons test. *: $p < 0.05$; **: $p < 0.01$;***: $p < 0.005$; ****: $p < 0.001$.

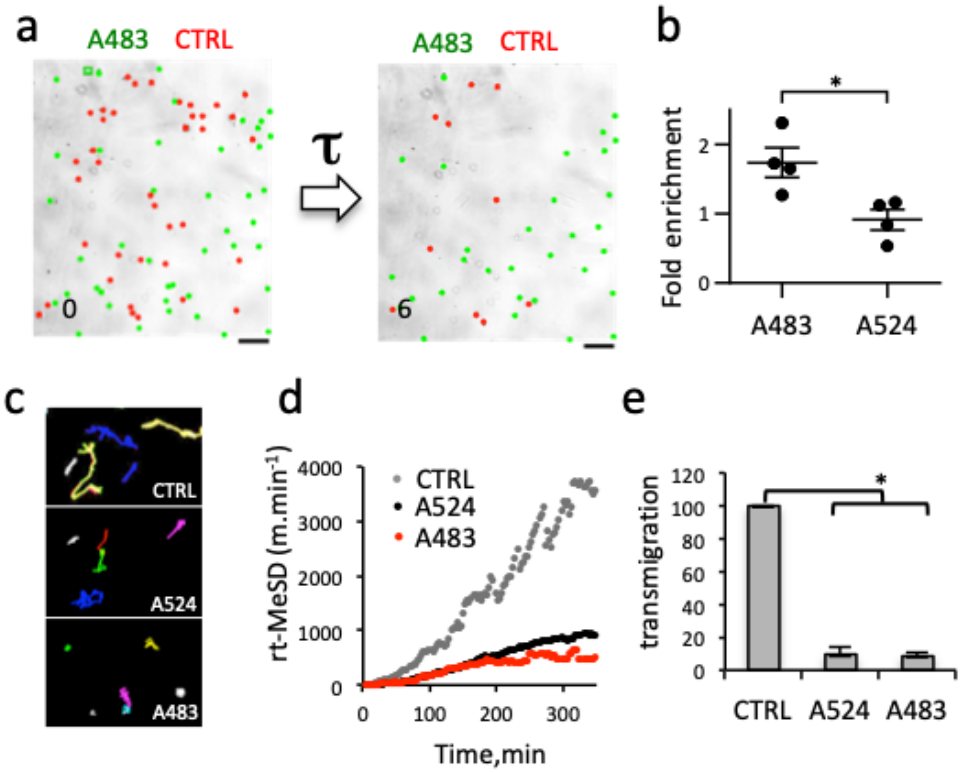


**Figure 4. A483-mediated vinculin supra-activation stimulates strong cell adhesion and inhibits tumor cell invasion.**

**a, b,** 1205Lu melanoma cells were transfected with the indicated constructs, labeled with calcein (methods) and mixed with the same ratio of control cells. Cells were perfused in a microfluidic chamber and allowed to adhere for 20 min prior to shear stress application. **a**, representative fields. The number indicates the elapsed time after shear stress application. **b**, Scatterplot of fold enrichment of: A483 (N = 4, n = 610) or A524 (N = 4, n = 433) transfected cells vs control cells (1594 cells, N = 4). Unpaired t test. *: p = 0.0229. **c, d,** cells were transfected with the indicated constructs, and analyzed by time-lapse videomicroscopy. **c**, representative single cell migration 20-hour tracks for indicated samples. **d**, Root of Median Square of displacement over time for control- (61 cells, N = 3), GFP-A524- (61 cells, N = 3) and GFP-A483 transfectants (64 cells, N = 3). ***p = 0.0007. The slopes were analyzed using a covariance test and found to be statistically different (ANCOVA, $p < 2x10^{-16}$). **e,** $5 \times 10^4$ cells were seeded in matrigel

314 chambers. The percent of transmigrated cells is indicated. (N = 3). Kruskal-Wallis test with Dunn's

315 multiple comparisons test. *: $p < 0.05$.

316

## METHODS

### Generation of constructs

Human vinculin constructs were generated by polymerase chain reaction using the forward primer 5' GCGCATATGCCAGTGTTTCATACG-3' and reverse primer 5'-CGTCGACTCACCAGGCATCTTCATCGGC-3' for D1 (residues 1-258) or 5'-CGTCGACTCAGTGTACAGCTGCTTTG-3' for D2 (residues 1-492) using a plasmid containing full-length octahistidine-tagged human vinculin (residues 1–1,066), as template[10], and cloned into the NdeI-SalI sites of pet15b (Novagen). The IpaA constructs GFP-A524 and GFP-A483 were generated by polymerase chain reaction (PCR) and cloning into pcDNA3.1 NT-GFP Topo TA (Invitrogen) using the 5'-TCAAAGGACATTACAAAATCC-3' and 5'-GCGATATCATGGCCAGCAAAGG-3' forward primers, respectively, and the 5'-GCGCGGCCGCTTAATCCTTATTGATATTC-3' reverse primer. The GST-A483A construct was generated by PCR using 5'-GGCGAATTCCCGGAGACACATATTTAACACG-3' forward and 5'-GCCGTCGACTTAATCCTTATTGATATTCT-3' reverse primers and cloning into the *EcoRI-SalI* ofpGEX-4T-2 (GE Lifesciences). pGST-A524 was previously described[24]. The pGFP-vD1 plasmid was generated by polymerase chain reaction using the forward primer 5'-ACCCGGGATCCCGCC-3' and reverse primer 5'-ACCCGGGACCAGGCA-3', and cloned into peGFP. The pmCherry-human vinculin (HV) and pmCherry-VASP plasmids were from Addgene. Stealth siRNA anti-human vinculin was from Invitrogen (reference number 1299001).

### Protein purification

BL21 (DE3) chemically competent *E. coli* (Life Technologies) was transformed with the expression constructs. D1 and D1D2 were purified essentially as described[11, 25]. For the IpaA derivatives, bacteria grown until $OD_{600nm}$ = 1.0 were induced with 0.5 mM IPTG and incubated for another 3 hrs. Bacteria were pelleted and washed in binding buffer 25 mM Tris PH 7.4, 100 mM NaCl and 1 mM beta-mercaptoethanol, containing Complete™ protease inhibitor. Bacterial pellets were resuspended in

1/50th of the original culture volume and lyzed using a cell disruptor (One shot model, Constant System Inc.). Proteins were purified by affinity chromatography using a GSTrap HP affinity column (GE Healthcare) and size exclusion chromatography (HiLoad S200, Ge Healthcare). Samples were stored aliquoted at -80°C at concentrations ranging from 1 to 10 mg/ml.

**Protein complex formation analysis**

Proteins were incubated at a concentration of 30 µM in binding buffer for 60 min at 4°C. Samples were analyzed by SEC-MALS (Wyatt Technology Europe) using a 24 ml Superdex 200 Increase 10/300 GL filtration column and a MiniDAWN TREOS equipped with a quasi-elastic light scattering module and a refractometer Optilab T-rEX (Wyatt Technology). Data were analyzed using the ASTRA 6.1.7.17 software (Wyatt Technology Europe). Protein complex formation was visualized by PAGE under non-denaturing conditions using à 7.5% polycrylamide gel, followed by Coomassie blue staining.

**Solid-phase binding assay**

96–well Maxisorp (Nunc) ELISA plates were coated with 30 nM of full-length vinculin, vinculin constructs or IpaA proteins at the indicated concentrations in binding buffer (25 mM Tris PH 7.4, 100 mM NaCl and 1 mM β-mercaptoethanol). Samples were blocked with PBS-BSA 2%, washed and incubated with IpaA or vinculin proteins in binding buffer containing 0.2% BSA at room temperature for one hour. After incubation, the plates were washed and incubated with an anti-IpaA (dilution 1/2000[e]) polyclonal primary antibody[3] or anti-vinculin (dilution 1/2000[e]) Vin11Vin.5 monoclonal antibody (Sigma-Aldrich) in binding buffer containing 0.2% BSA for one hour at room temperature. Plates were washed and incubated with an HRP-coupled secondary anti-rabbit or anti-mouse IgG antibody (1/32000[e]) (Jackson ImmunoResearch) for one hour. The reaction was revealed by adding 100 µl of tetramethylbenzidine (Sigma-Aldrich) for 15 min, stopped by adding 50 µl of 0.66N $H_2SO_4$ and the absorbance was read at 450 nm (Dynatech MR400).

**BN-PAGE (Blue Native – Polyacrylamide Gel Electrophoresis) protein native gel analysis and complex cross-linking**

25 µM of vinculin constructs were incubated with different molar ratios of IpaA proteins in a 1X BN-PAGE buffer (250 mM ε-aminicaprionic acid and 25mM Bis-Tris PH 7,0) at 4°C for one hour. The protein mixtures were separated in a one-dimension native BN-PAGE electrophoresis as described[26]. For vinculin-IpaA protein ratio assay, vinculin-IpaA bands containing the complexes separated by BN-PAGE were cut, sliced and boiled in 2 x Laemmli SDS buffer followed by SDS-PAGE. The second dimension SDS-PAGE gels were stained (colloidal Coomassie staining) and the density of the bands was determined using Image J. The normalized vinculin:IpaA ratio of the complexes was compared using a non-parametric Kruskal-Wallis rank sum test (R statistical software).

For crosslinking vinculin-IpaA complex, bands containing the complexes were cut, sliced and electroeluted in native conditions (15 mM Bis-Tris pH 7.0 and 50 mM Tricine) inside a closed dialysis membrane (SpectraPor). The soluble complexes were recovered and their buffer exchanged twice into an amine-free cross-link buffer in 25 mM HEPES pH 7.0 containing 100 mM NaCl using 10MWCO ZEBA desalting columns (Thermo Scientific). The fractions containing the complexes were incubated for 1 hr at 4°C with 10 mM N-hydroxysulfosuccinimide and 5 mM EDC (Sigma-Aldrich) following the manufacturer's recommendations. The cross-linking reaction was stopped by adding 50 mM Tris pH 7.4 and incubating for 20 minutes. Samples were denaturated in 2x SDS Laemmli buffer for 5 min at 95°C and complexes were eluted from gel slices following SDS-PAGE.

**Liquid Chromatography Mass spectrometry (LC-MS)**

Complexes obtained after the cross-linking step were loaded onto a 4-20% polyacrylamide gradient gels and Coomassie stained. The bands containing the complexes were cut and submitted to tryptic digestion[27]. The experiments were performed in duplicates for the 3 complexes D1:A524, D1D2:A524 and D1D2:A483. Peptides obtained after tryptic digestion were analyzed on a Q Exactive Plus instrument (Thermo Fisher Scientific, Bremen) coupled with an EASY nLC 1 000 chromatography system (Thermo

Fisher Scientific, Bremen). Sample was loaded on an in-house packed 50 cm nano-HPLC column (75 µm inner diameter) with C18 resin (1.9 µm particles, 100 Å pore size, Reprosil-Pur Basic C18-HD resin, Dr. Maisch GmbH, Ammerbuch-Entringen, Germany) and equilibrated in 98 % solvent A (H2O, 0.1 % FA) and 2 % solvent B (ACN, 0.1 % FA). A 120 minute-gradient of solvent B at 250 nL.min-1 flow rate was applied to separate peptides. The instrument method for the Q Exactive Plus was set up in DDA mode (Data Dependent Acquisition). After a survey scan in the Orbitrap (resolution 70 000), the 10 most intense precursor ions were selected for HCD fragmentation with a normalized collision energy set up to 28. Charge state screening was enabled, and precursors with unknown charge state or a charge state of 1 and >7 were excluded. Dynamic exclusion was enabled for 35 or 45 seconds respectively.

**Data analysis**

The identification of cross-linked peptides from LC-MS data was performed using SIM-XL v. 1.3[28], with the following search parameters: EDC as cross-linker, a tolerance of 20 ppm for precursor and fragment ions, trypsin fully specific digestion with up to three missed cleavages. Carbamidomethylation of cysteines was considered as a fixed modification. All initial identification of cross-linked peptides required a primary score of SIM-XL greater than 2.5 for inter-links and 2.0 for intra-links or loop-links. As single incorrect cross-link identification might lead to a different model, a manual post-validation of the search engine results at the MS2 level was thus performed. A 2D-map showing the protein-protein interaction was generated as an output (Figs. 2a,b). Only peptides present in the 2 replicates are gathered in Supplementary Tables 1-3 and were used for the modeling.

**Modeling**

We used the constraints obtained from the cross-linking MS data (Suppl. Tables 1-3) to guide the protein structure modeling using the TX-MS protocol as described by Hauri, Khakzad et al.[29]. In short, TX-MS uses the Rosetta comparative modeling protocol (RosettaCM)[30], and the flexible backbone docking protocol (RosettaDock)[31] to generate models and evaluate how well each model explains the MS constraints using a novel scoring function. Here, a total of 100,000 models was generated, of which the

highest-scoring model is displayed in (Fig2e), supported by a total of 100 inter and intra-molecular cross-links.

**Cell lines**

C2.7 myoblasts[32] and MEF vinculin null cells[8] were routinely grown in DMEM 1 g / L glucose containing 10 % FCS in a 37°C incubator containing 10 % $CO_2$. 1205Lu melanoma cells[33] were grown in RPMI + Glutamax medium (RPMI1640) supplemented with 10 % fetal calf serum (FCS) and non-essential aminoacids in a 37°C incubator with 5 % $CO_2$.

**Immunofluorescence staining**

C2.7 mice myoblasts cells were seeded at $2.5x10^4$ cells in 25 mm-diameter coverslips. Cells were transfected with 3 µg of pGFP-A524 or pGFP-A483 plasmids with 6 µl JetPEI transfection reagent (Polyplus) for 16 hours following the manufacturer's recommendations. Cells were fixed in PBS containing 3.7% paraformaldehyde for 20 min at 21°C and permeabilized with 0.1% Triton X-100 for 4 min at 21°C. Cells were processed for immunofluorescence staining using the Vin11.5 anti-vinculin monoclonal antibody (ref. V4505, Sigma-Aldrich) and anti-mouse IgG antibody coupled to Alexa 546 (Jackson Research) and Phalloidin-Alexa 633 (Invitrogen), as described previously[3]. Samples were analyzed using an Eclipse Ti inverted microscope (Nikon) equipped with a 60 x objective, a CSU-X1 spinning disk confocal head (Yokogawa), and a Coolsnap HQ2 camera (Roper Scientific Instruments), controlled by the Metamorph 7.7 software.

**TIRF (Total Internal Reflection Microscopy) analysis**

C2.7 cells were transfected with pmCherry-HV or pmCherry-VASP and the indicated plasmids as described above. Samples were mounted onto a TIRF microscopy chamber on a stage of an Eclipse Ti inverted microscope (Nikon) equipped with an Apo TIRF 100 x N.A. 1.49 oil objective heated at 37°C. TIRF analysis was performed using the Roper ILAS module and an Evolve EM-CCD camera (Roper Scientific

Instruments). When mentioned, Y-27632 was used at 100 µM. Image acquisition was performed every 12.5 seconds for 30 to 90 minutes.

**Live cell tracking**

1205Lu melanoma cells were transfected with IpaA constructs or GFP alone (control) and transferred in microscopy chamber on a 37°C 5%-$CO_2$ stage in RPMI1640 medium containing 25 mM HEPES. For cell tracking, samples were analyzed using and inverted Leica DRMIBe microscope and a 20 X phase contrast objective. Image acquisitions were performed every 3 min for 200 hrs. The mean velocity of migration was measured for all tracks followed for at least 5 hours. The root square of MdSD over time was plotted over time and fitted by linear regression. The slopes of the linear fit were compared using an ANCOVA test (linear model). The median cell surface was quantified as the mean of the surface for three time points (25%, 50% and 75%) of the whole cell track and dispersion measured by the Median absolute dispersion (MAD).

**Invasion assays**

Tissue culture Transwell inserts (8 µm pore size; Falcon, Franklin Lakes, NJ) were coated for 3 hours with 10 µg of Matrigel following the manufacturer's instructions (Biocoat, BD Biosciences, San Jose, CA). Inserts were placed into 24-well dishes containing 500 µl of RPMI medium supplemented with 1% fetal calf serum. $5 \times 10^4$ melanoma cells were added to the upper chamber in 250 µls of serum-free RPMI medium. After 24 hours, transmigrated cells were scored by bright field microscopy. Experiments were performed at least three times, each with duplicate samples.

**Image processing and statistical analysis**

For the quantification of the number of adhesion structures in C2.7 cells, a semi-automated protocol was developed using Icy software[34]. Spinning-disk fluorescent microscopy planes were used to detect vinculin structures using HK means thresholding and overlaid binary masks obtained from the threshold projections of F-actin labeled images (Max-entropy method). FAs were detected as spots

positive for both vinculin mCherry and actin structures using Wavelet Spot Detector. The number of adhesions was analyzed using Dunn's multiple comparisons test. The statistical analysis of cell motility was performed in the R software. Medians were compared using a Wilcoxon rank sum test and dispersion by Median absolute dispersion (MAD) parameter.

**Microfluidics cell adhesion assay**

Analysis of cell detachment under shear stress was based on previous works[35]. 1205Lu melanocytes were transfected with the indicated constructs, then labeled with 2 µ calcein-AM (Life Technologies) in serum-free DMEM for 20 minutes. Cells were detached by incubation with 2 µ Cytochalasin D (Sigma-Aldrich) for 40 minutes to disassemble FAs, followed by incubation in PBS containing 10 mM EDTA for 20 minutes. Cells were washed in EM buffer (120 mM NaCl, 7 mM KCl, 1.8 mM $CaCl_2$, 0.8 mM $MgCl_2$, 5 mM glucose and 25 mM HEPES at pH 7.3) by centrifugation and resuspended in the same buffer at a density of 1.5 x $10^6$ cells/ml. Calcein-labeled transfected cells and control unlabeled cells were mixed at a 1:1 ratio and perfused onto a 25 mm-diameter glass coverslips (Marienfeld) previously coated with 20 µg/ml fibronectin and blocked with PBS containing 2% BSA (Sigma-Aldrich) in a microfluidic chamber on a microscope stage at 37°C. We used a commercial microfluidic setup (Flow chamber system 1C, Provitro) and a Miniplus3 peristaltic pump (Gilson) to adjust the flow rate in the chamber. Microscopy analysis was performed using a LEICA DMRIBe inverted microscope equipped with a Cascade 512B camera and LED source lights (Roper Instruments), driven by the Metamorph 7.7 software (Universal imaging). Cells were allowed to settle for the indicated time prior to application of a 4 ml/min, flow corresponding to a wall shear stress of 22.2 dyn/$cm^2$ (2.22 Pa). Acquisition was performed using a 20 X objective using phase contrast and fluorescence illumination (excitation 480 ± 20 nm, emission 527 ± 30 nm). Fluorescent images were acquired before and after flushing to differentiate between target and control cells. Phase contrast images were acquired every 200 ms. Fold enrichment was defined as the ratio between of attached labeled and unlabeled cells.

**REFERENCES TO METHODS**

24 Ramarao, N. *et al.* Capping of actin filaments by vinculin activated by the Shigella IpaA carboxyl-terminal domain. *FEBS letters* **581**, 853-857, doi:10.1016/j.febslet.2007.01.057 (2007).

25 Papagrigoriou, E. *et al.* Activation of a vinculin-binding site in the talin rod involves rearrangement of a five-helix bundle. *The EMBO journal* **23**, 2942-2951, doi:10.1038/sj.emboj.7600285 (2004).

26 Eubel, H. & Millar, A. H. Systematic monitoring of protein complex composition and abundance by blue-native PAGE. *Cold Spring Harb Protoc*, pdb prot5221, doi:10.1101/pdb.prot5221 (2009).

27 Shevchenko A, Tomas H, Havlis J, Olsen JV, Mann M. Nat Protoc. In-gel digestion for mass spectrometric characterization of proteins and proteomes. **1**(6):2856-60 (2006).

28 Lima, D. B. et al. SIM-XL: A powerful and user-friendly tool for peptide cross-linking analysis. J Proteomics **129**, 51-55, doi:10.1016/j.jprot.2015.01.013 (2015).

29 Hauri, S., Khakzad, H., Happonen, L., Teleman, J., Malmström, J., & Malmström, L. Rapid determination of quaternary protein structures in complex biological samples. Nature communications, **10**(1), 192. doi:10.1038/s41467-018-07986-1 (2019).

30 Song, Y. *et al.* High-resolution comparative modeling with RosettaCM. *Structure* **21**, 1735-1742, doi:10.1016/j.str.2013.08.005 (2013).

31 Gray, J. J. High-resolution protein-protein docking. *Current opinion in structural biology* **16**, 183-193, doi:10.1016/j.sbi.2006.03.003 (2006).

32 Mitrossilis, D. et al. Single-cell response to stiffness exhibits muscle-like behavior. *Proc. Nat. Acad. Sci USA.* **106**(43), 18243-18248; https://doi.org/10.1073/pnas.0903994106 (2009).

33 Smalley, K. S., et al. Increased cyclin D1 expression can mediate BRAF inhibitor resistance in BRAF V600E-mutated melanomas. *Mol Cancer Ther.,* **7**(9):2876-83. doi: 10.1158/1535-7163.MCT-08-0431 (2008).

34 de Chaumont, F. *et al.* Icy: an open bioimage informatics platform for extended reproducible research. *Nat Methods* **9**, 690-696, doi:10.1038/nmeth.2075 (2012).

511 35 Gutierrez, E. *et al.* Microfluidic devices for studies of shear-dependent platelet adhesion. *Lab*

512 *Chip* **8**, 1486-1495, doi:10.1039/b804795b (2008).

513

514

# SUPPLEMENTARY INFORMATION

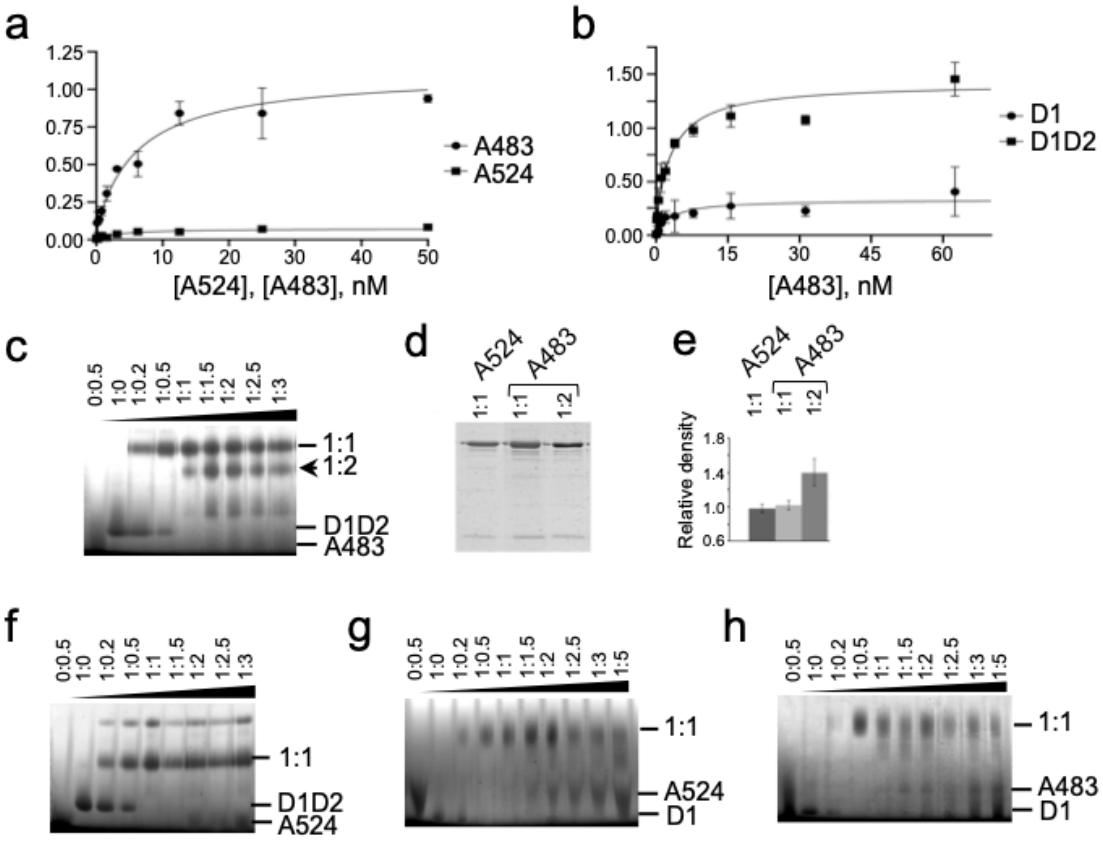


**Supplementary Fig. 1. IpaA VBS3 reveals multiple binding sites on vinculin.**

**a, b,** Solid phase binding assays. **a,** coating: HV; ligands: A483 (solid circles); A524 (solid squares). **b,** coating: D1 (solid circles) or HVD1D2 (solid squares); ligand: A483. **c, f-h,** BN-PAGE in 6-18% polyacrylamide gradient gels and Coomassie staining analysis of D1D2:A483 (**c**), D1D2:A524 (**f**), D1:A524 (**g**) or D1:A483 (**h**) complexes. The molar ratio is indicated above each lane. Arrowheads indicate protein alone, or complex migration at the indicated molar ratio. **d**, bands were recovered from BN-PAGE and analyzed in a second dimension SDS-PAGE in a 15% polyacrylamide gel and Coomassie staining. Bands were analyzed by densitometry. **e**, ratio of density values for the A524-D1D2 complex (empty bar) and A483-D1D2 complexes corresponding to the upper (light grey bar) or lower (dark grey bar) shifts.

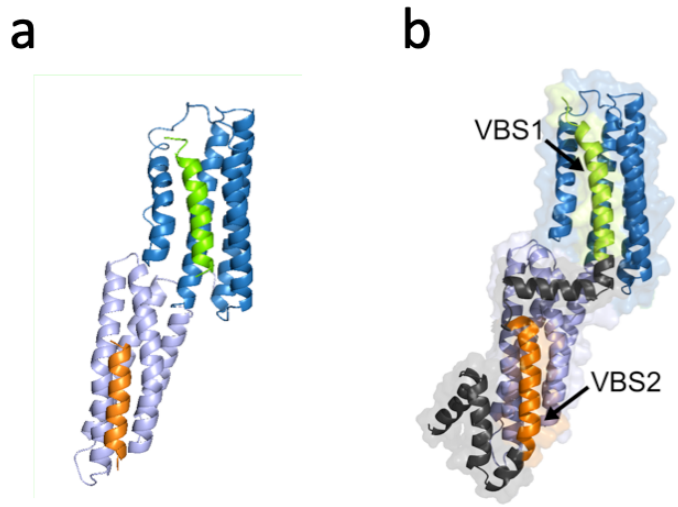


**Supplementary Figure 2. Structural models of vD1:A524. a,** Structure predicted from the resolved vD1:IpaA VBS1: and vD1:IpaA VBS2 crystal structures[11, 12]**. b,** Structural model of vD1:A524. The model was established using RosettaCM protocol and accounts for 19 inter and intra-molecular cross-links out of 24 identified (Suppl. Table 1).

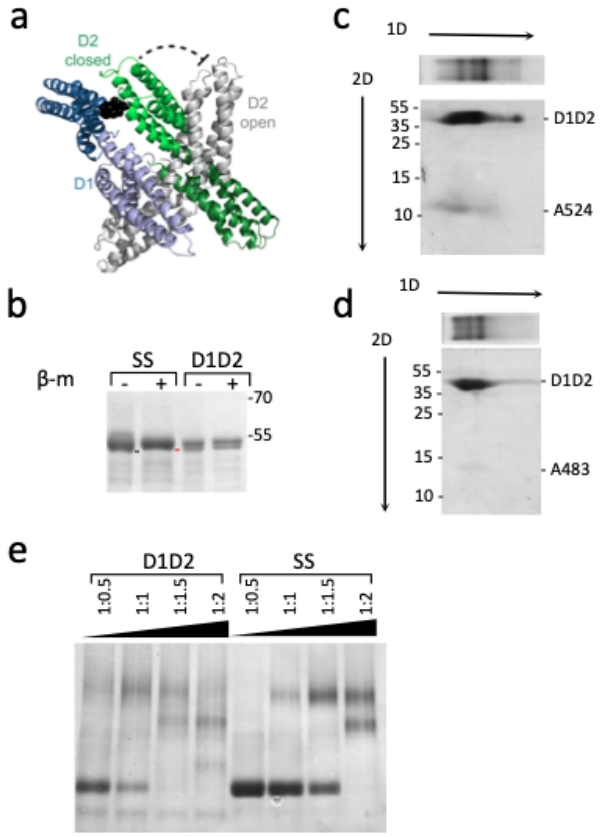


536

537

538 **Supplementary Figure 3. Cysteine-clamped vinculin D1D2 does not form high order complexes.** **a**,
539 Structural model of cystein-clamped vinculin. Blue: D1 domain. Green: D2 domain in the closed
540 conformer. Grey: D2 domain in the open conformer. Black: C68-C396 cystein clamp preventing the
541 switch from closed to open conformers. **b-e**, Coomassie blue staining. **b**, Disulfide bridge formation in
542 D1D2. D1D2: wild-type sequence. SS: D1D2 Q68C A396C. SDS-PAGE analysis using a 10 % polyacrylamide
543 gel. + β-metOH: samples were boiled in Laemmli sample loading buffer containing 5 mM beta-
544 mercaptoethanol prior to SDS-PAGE. The molecular weight markers in kDa are indicated. The black and
545 red bars point the respective migration of unreduced and reduced D1D2 Q68C A396C, respectively. **c**, **d**,
546 gel strips of the native-PAGE corresponding to the A524 + D1D2 (**c**) or A483 + D1D2 (**d**) as shown in **Fig.**
547 **1e** were analyzed in a second dimension by SDS-PAGE using a 10 % polyacrylamide gel as depicted.
548 D1D2, SS, A483 and A524 are indicated. **e**, BN-PAGE analysis in a 6-18% polyacrylamide gradient gel of

549 D1D2:A483 (D1D2) and SS:A483 (SS) complexes. The molar ratio is indicated above each lane.

550 Arrowheads indicate protein alone, or complex migration

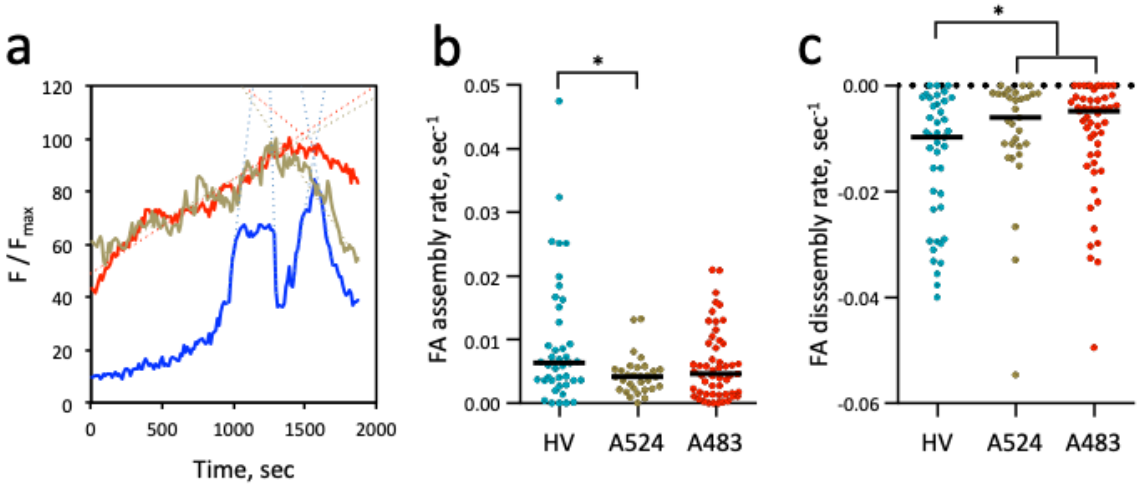


551

552 **Supplementary Figure 4. TIRF analysis of FA dynamics.** C2. 7 cells were transfected with HV-mCherry

553 (HV), HV-mCherry and GFP-A524 (A524) or HV and GFP-A483 (A483). The dynamics of HV-mCherry-

554 labeled FAs were analyzed by TIRF microscopy. **a**, traces correspond to the variations of average

555 fluorescence intensity of a representative single FA (F) normalized to its maximal average fluorescence

556 intensity over the analyzed period in seconds ($F_{max}$). Blue: HV; green: HV+A524; red: HV+A483. **b**, **c**,

557 instant assembly (**b**) or disassembly (**c**) rates were inferred from the slopes of linear fits as depicted in a),

558 with a Pearson correlation value > 0.85. HV: n = 41, N = 3; HV+A524: n = 31, N = 2; HV+A483: n = 55, N =

559 3. Mann-Whitney U test. *: $p < 0.05$

560

561

562

563

564

565

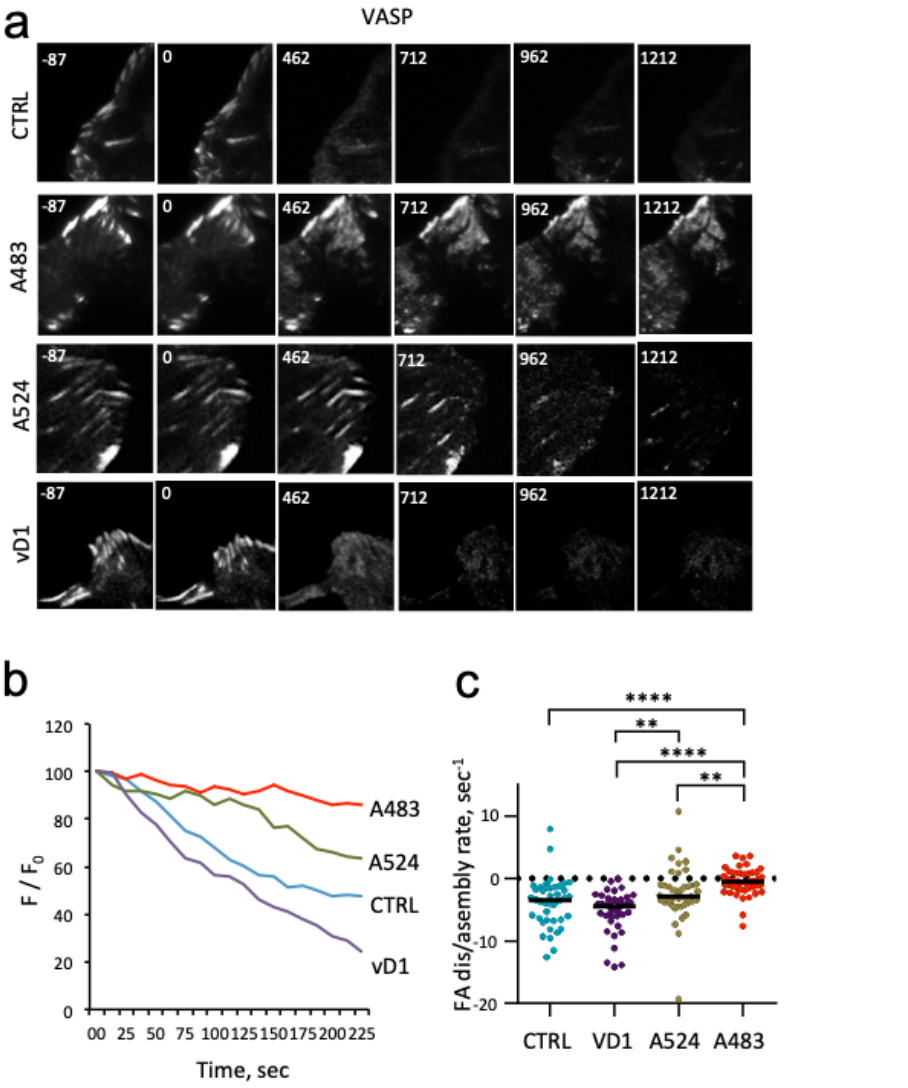


**Supplementary Figure 5. A483 stabilizes VASP-containing cell adhesions in the absence of mechanotransduction**

TIRF microscopy of C2.7 cells transfected with mCherry-VASP alone (CTRL) or co-transfected with GFP-A524 (A524), GFP-vD1 (vD1), or GFP-A483 (A483). Adhesion kinetic parameters were determined from time-lapse acquisitions of cells co-transfected with mCherry-VASP and the indicated construct following treatment with 100 µM Y-27632. **a**) Representative time series acquisitions. Numbers indicated the elapsed time in seconds, with the inhibitor added at t = 0. Scale bar = 5 µm. **b**, $\Delta F/F_0$: normalized average fluorescence intensity of adhesions as a function of time. Representative traces corresponding to single adhesions for the indicate samples. **c**, initial rates of adhesion disassembly inferred from linear

fits. N = 4. Number of adhesions analyzed: CTRL: 42; A483: 43; A524: 40; vD1: 40. Dunn's multiple comparisons test. *: $p < 0.05$; ****: $p < 0.001$.

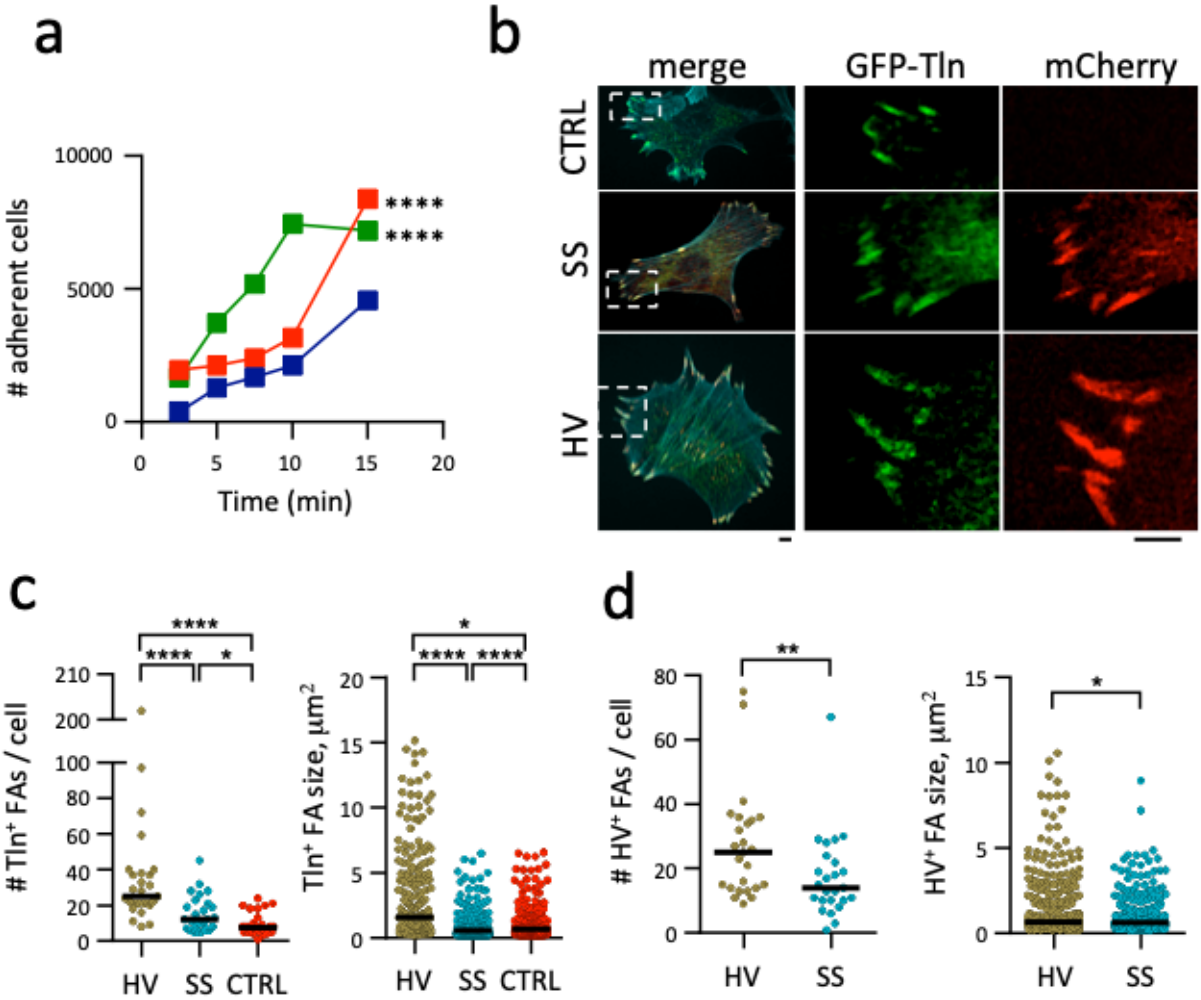


**Supplementary Figure 6. Effects of A483 and vinculin supra-activation on cell adhesion kinetics**

**a**, 1205Lu melanoma cells were transfected with GFP alone (blue), GFP-A524 (red) or GFP-A483 (green), lifted up by trypsinization and plated for the indicated time on Fn-coated coverslips. Samples were washed, fixed and adherent cells were scored microscopically. The total number of adherent cells scored is indicated. GFP: 3223 cells, N = 4; GFP-A524: n=7418, N = 4; GFP-A483: n = 5668, N = 4. Chi square corrected with Bonferroni mutliple comparison correction. ****: $p < 0.001$. **b-d**, MEF vinculin null cells were co-transfected with GFP-talin (CTRL) and full length vinculin-mCherry (HV) or HV Q68C A396C-mCherry (SS). Samples were fixed and processed for fluorescence staining of F-actin. **b,** Representative fluorescence micrographs. Red: Vinculin-mCherry; green:

596 GFP-talin; cyan: F-actin. Scale bar = 1 µm. **c**, **d**, FAs were scored using a semi-automatic detection program
597 (Methods) and their number per cell (left) and size (right) are shown. Bar: median size. FAs labeled with: **c**,
598 GFP-talin; **d**, HV or SS. CTRL: n=28, N=3; HV: n = 25 , N = 3; SS: n = 25, N = 3. Mann-Whitney test with
599 Bonferroni multiple comparison correction. * p<0.05; ** p<0.01; *** p<0.005; **** p<0.001.

600

601

602

603

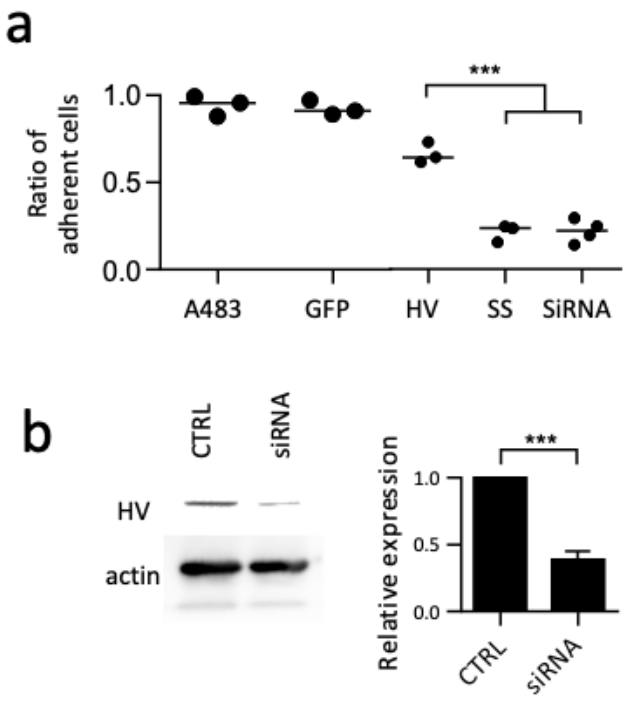


604

605 **Supplementary Figure 7. Role of vinculin supra-activation on cell adhesion.**

606 **a,** 1205Lu melanoma cells were transfected with the indicated constructs, labeled with calcein (methods) and
607 mixed with the same ratio of control cells. Cells were perfused in a microfluidic chamber and allowed to
608 adhere for 30 min (large solid circles) or 15 min (small solid circles) prior to shear stress application. Scatterplot
609 of the ratio of adherent cells: A483 (N = 3, n = 557); GFP (N = 3, n = 490); HV: vinculin mCherry (N = 3, n = 481);

610 SS: vinculin Q68C A396C-mCherry (N = 3, n = 259); siRNA: cells treated with anti-vinculin siRNA (N = 3, n = 395).

611 Unpaired t test. ***: $p < 0.005$. **b**, 1205Lu melanoma cells were mock-transfected (CTRL) or treated with anti-

612 vinculin siRNA (siRNA, Methods). Right: anti-vinculin Western blot analysis. Left: average HV band intensity

613 normalized to that of control cells. Unpaired t test. ***: $p = 0.005$.

614

615 **SUPPLEMENTARY TABLES**

616

| # | Exp. $MH^+$ | Primary Score | Peptide Sequence | A524 | Hv D1 |
|---|---|---|---|---|---|
| 32670 | 4457.1 | 3.28 | IDDTSAELLTDDISDLKNNN**D**ITAENNNIYK - MA**K**MIDER | D604 | K173 |
| 32798 | 1924.16 | 2.61 | INN**K**LK - **E**LLPVLISAMK | K540 | E200 |
| 33042 | 4613.23 | 3.70 | IDDTSAELLT**D**DISDLKNNNDITAENNNIYK - NLGPGMT**K**MAK | D594 | K170 |
| 33042 | 4613.23 | 3.70 | IDDTSAELLTD**D**ISDLKNNNDITAENNNIYK - NLGPGMT**K**MAK | D595 | K170 |
| 33042 | 4613.23 | 4.11 | IDDTSAELLTDDISDLKNNN**D**ITAENNNIYK - NLGPGMT**K**MAK | D604 | K170 |
| 33322 | 5310.64 | 4.48 | IDDTSAELLTDDISDL**K**NNNDITAENNNIYK - VGKETVQTTE**D**QILKR | K600 | D67 |
| 33334 | 2347.28 | 2.51 | DVTTSLS**K**VLK - MSA**E**INEIIR | K625 | E240 |
| 33432 | 2138.26 | 2.88 | VL**K**NINKD - **E**LLPVLISAMK | K628 | E200 |
| 33496 | 2315.32 | 3.09 | AA**K**DVTTSLSK - **E**LLPVLISAMK | K617 | E200 |
| 34822 | 2642.55 | 2.68 | AKEVSSALS**K**VLSK - **E**LLPVLISAMK | K579 | E200 |
| 38218 | 3685.86 | 3.87 | NIN**K**D - TIESILEPVAQQISHLVIMHEEG**E**VDGK | K632 | E31 |
| 38218 | 3685.86 | 3.66 | NIN**K**D - TIESILEPVAQQISHLVIMH**E**EGEVDGK | K632 | E28 |
| | | | | | |
| # | Exp. $MH^+$ | Primary Score | Peptide Sequence | Hv D1 | |
| 34075 | 2342.29 | 3 | **E**LLPVLISAMK - NLGPGMT**K**MAK | E200 | K170 |

| | | | | | |
|---|---|---|---|---|---|
| 36135 | 3088.67 | 2.62 | NFTVE**K**MSAEINEIIR - **E**LLPVLISAMK | K236 | E200 |
| | | | | | |
| **#** | **Exp. MH$^+$** | **Primary Score** | **Peptide Sequence** | **A524** | |
| 14281 | 3051.56 | 3.52 | NYVT**E**TNADTIDKNHAIYEK - INN**K**LK | E554 | K540 |
| 15477 | 3342.67 | 2.74 | NYVT**E**TNADTIDKNHAIYEK - A**K**EVSSALSK | E554 | K571 |
| 17603 | 3141.54 | 2.71 | NYVTETNADTID**K**NHAIYEK - **E**VSSALSK | K562 | K572 |
| 31359 | 4483.2 | 2.64 | IDDTSA**E**LLTDDISDLKNNNDITAENNNIYK - A**K**EVSSALSK | E590 | K571 |
| 31996 | 2965.5 | 2.94 | IDDTSAELLTDDIS**D**LK - AA**K**DVTTSLSK | D598 | K617 |
| 31996 | 2965.5 | 2.51 | IDDTSAELLT**D**DISDLK - AA**K**DVTTSLSK | D594 | K617 |
| 32705 | 4586.24 | 4.1 | IDDTSAELLTDDISDLKNNNDITA**E**NNNIYK - AA**K**DVTTSLSK | E608 | K617 |
| 33253 | 3291.74 | 3.81 | IDDTSAELLTD**D**ISDLK - AKEVSSALS**K**VLSK | D595 | K579 |
| 33997 | 5328.54 | 4.76 | IDDTSAELLTDDISDL**K**NNNDITAENNNIYK - ID**D**TSAELLTDDISDLK | K600 | D586 |
| 34007 | 4655.33 | 4.78 | IDDTSAELLT**D**DISDLKNNNDITAENNNIYK - DVTTSLS**K**VLK | D594 | K625 |

**Suppl. Table 1**. Cross-linked residues characterized in the D1:A524 complex (XL-amino acids of each protein are bolded in the sequences).

| # | Exp. MH$^+$ | Primary | Peptide Sequence | A524 | Hv D1D2 |
|---|---|---|---|---|---|

| | | Score | | | |
|---|---|---|---|---|---|
| 20480 | 3470.68 | 3.86 | NYVT**E**TNADTIDKNHAIYEK - NLGPGMT**K**MAK | E554 | K170 |
| 23021 | 3883.92 | 3.71 | NYVTETNADTID**K**NHAIYEK - **E**TVQTTEDQILKR | K562 | E60 |
| 24707 | 3117.73 | 5.00 | AKEVSSALSKVLSK - VGKETVQTT**E**DQILK | K579 | E66 |
| 36724 | 4612.22 | 4.82 | IDDTSAELLTDDISDLKNNN**D**ITAENNNIYK - NLGPGMT**K**MAK | D604 | K170 |
| 39712 | 5255.49 | 3.79 | IDDTSAELLTDDIS**D**LKNNNDITAENNNIYK - NLGPGMTKMA**K**MIDER | D598 | K173 |
| 39893 | 5162.6 | 4.51 | IDDTSA**E**LLTDDISDLKNNNDITAENNNIYK - ALA**K**QVATALQNLQTK | E590 | K464 |
| 40011 | 2641.56 | 4.45 | AKEVSSALS**K**VLSK - **E**LLPVLISAMK | K579 | E200 |
| 41002 | 3047.64 | 3.99 | L**K**VTDANIR - GILSGTSDLLLTFD**E**AEVR | K542 | E128 |
| 41440 | 3944.01 | 3.86 | IDDTSAELLTDDIS**D**LK - AQQVSQGLDVLTA**K**VENAAR | D598 | K366 |
| 42699 | 3685.87 | 4.03 | NIN**K**D -TIESILEPVAQQISHLVIMHEEG**E**VDGK | K632 | E31 |
| | | | | | |
| **#** | **Exp. MH$^+$** | **Primary Score** | **Peptide Sequence** | **Hv D1D2** | |
| 25162 | 3323.71 | 4.54 | LNQA**K**GWLRDPSASPGDAGEQAIR - ALASI**D**SK | K281 | D274 |
| 30025 | 3169.64 | 4.03 | GQGSSPVAMQ**K**AQQVSQGLDVLTAK - V**E**NAAR | K352 | E368 |
| 30045 | 3278.66 | 3.69 | VLQLTSWDE**D**AWASK - **K**LEAMTNSKQSIAK | D275 | K381 |
| 30201 | 3695.87 | 3.82 | LNQA**K**GWLRDPSASPGDAGEQAIR - MSA**E**INEIIR | K281 | E240 |
| 31264 | 3251.77 | 5.03 | ALA**K**QVATALQNLQTKTNR - RQGKGDSP**E**AR | K464 | E458 |
| 31264 | 3251.77 | 4.50 | ALA**K**QVATALQNLQTKTNR - RQGKG**D**SPEAR | K464 | D455 |

| | | | | | |
|---|---|---|---|---|---|
| 31620 | 2516.36 | 3.44 | ALASIDS**K**LNQAK - MSA**E**INEIIR | K295 | E240 |
| 35256 | 3787.88 | 4.12 | GILSGTSDLLLTFD**E**AEVR - GSSHHHHHHSS**G**LVPR | E128 | G12 |
| 38115 | 3310.75 | 4.29 | GILSGTSDLLLTFD**E**AEVR - AVANSRPA**K**AAVH | E147 | K507 |
| 39508 | 3685.90 | 3.56 | GQGSSPVAMQ**K**AQQVSQGLDVLTAK - MSA**E**INEIIR | K352 | E240 |
| 40134 | 3129.61 | 2.19 | NQGIEEALKNRNFTVEKMSAEINEIIR | E224 | K236 |
| 40285 | 3184.71 | 4.81 | AQQVSQGLDVLTA**K**VENAAR - SLG**E**ISALTSK | K366 | E437 |
| 40296 | 2280.32 | 3.69 | **E**LLPVLISAMK - LNQA**K**GWLR | E200 | K281 |
| 40351 | 3255.72 | 4.00 | AQQVSQGLDVLTA**K**VENAAR - MSA**E**INEIIR | K366 | E240 |
| 40571 | 4536.51 | 4.44 | G**D**SPEARALAKQVATALQNLQTK - SLGEISALTS**K**LADLRRQGK | D455 | K444 |
| 40881 | 3704.92 | 4.32 | **K**IDAAQNWLADPNGGPEGEEQIR - **E**LLPVLISAMK | K387 | E200 |
| 40923 | 3100.63 | 3.94 | AQQVSQGLDVLTAKV**E**NAAR - **K**LEAMTNSK | E368 | K373 |
| 41473 | 3723.01 | 4.34 | GQGSSPVAMQ**K**AQQVSQGLDVLTAK - **E**LLPVLISAMK | K352 | E200 |
| 41482 | 4633.41 | 3.54 | TI**E**SILEPVAQQISHLVIMHEEGEVDGK - **K**LEAMTNSKQSIAK | E28 | K381 |
| 42201 | 3294.83 | 3.66 | AQQVSQGLDVLTA**K**VENAAR - **E**LLPVLISAMK | K366 | E200 |
| | | | | | |
| **#** | **Exp. MH$^+$** | **Primary Score** | **Peptide Sequence** | **A524** | |
| 15424 | 3050.56 | 3.57 | NYVT**E**TNADTIDKNHAIYEK - INN**K**LK | E554 | K540 |
| 16531 | 3340.67 | 3.55 | NYVTETNA**D**TIDKNHAIYEK - A**K**EVSSALSK | E558 | K571 |

| | | | | | |
|---|---|---|---|---|---|
| 16865 | 3341.67 | 4.11 | NYVT**E**TNADTIDKNHAIYEK - A**K**EVSSALSK | E554 | K571 |
| 34602 | 4584.25 | 4.05 | IDDTSA**E**LLTDDISDLKNNNDITAENNNIYK - AA**K**DVTTSLSK | E590 | K617 |
| 35202 | 4586.25 | 5.2 | IDDTSAELLTDDISDLKNNN**D**ITAENNNIYK - AA**K**DVTTSLSK | D594 | K617 |
| 35824 | 4583.26 | 3.43 | IDDTSAELLTDDISDLKNNNDITA**E**NNNIYK - AA**K**DVTTSLSK | E608 | K617 |
| 39340 | 4911.48 | 4.37 | IDDTSAELLTD**D**ISDLKNNNDITAENNNIYK - AKEVSSALS**K**VLSK | D595 | K579 |
| 39340 | 4911.48 | 4.06 | IDDTSAELLTDDIS**D**LKNNNDITAENNNIYK - AKEVSSALS**K**VLSK | D598 | K579 |
| 39340 | 4911.48 | 3.83 | IDDTSA**E**LLTDDISDLKNNNDITAENNNIYK - AKEVSSALS**K**VLSK | E590 | K579 |
| 39730 | 3291.74 | 3.64 | IDDTSAELLTD**D**ISDLK - A**K**EVSSALSKVLSK | D595 | K571 |
| 40244 | 4655.32 | 4.35 | IDDTSAELLT**D**DISDLKNNNDITAENNNIYK - DVTTSLS**K**VLK | D594 | K625 |
| 40244 | 4655.32 | 4.35 | IDDTSAELLTD**D**ISDLKNNNDITAENNNIYK - DVTTSLS**K**VLK | D595 | K625 |

**Suppl. Table 2**. Cross-linked residues characterized in the D1D2:A524 complex (XL-amino acids of each protein are bolded in the sequences).

632

633

634

635

636

| # | Exp. $MH^+$ | Primary Score | Peptide Sequence | A483 | Hv D1D2 |
|---|---|---|---|---|---|
| 13237 | 3014.59 | 3.29 | DIT**K**STTEHR - VGK**E**TVQTTEDQILKR | K530 | E66 |
| 14671 | 2518.38 | 2.49 | SKDIT**K** - VGK**E**TVQTTEDQILKR | K526 | E66 |
| 14791 | 2556.44 | 2.35 | INN**K**LK - VGK**E**TVQTTEDQILKR | K540 | E66 |
| 17806 | 2621.29 | 3.10 | **G**SPGIPGDTYLTR - QQ**E**LTHQEHR | G517 | E181 |
| 20039 | 2571.40 | 3.08 | L**K**VTDANIR **-** **E**TVQTTEDQILKR | K542 | E66 |
| 20526 | 3651.79 | 3.37 | NYVT**E**TNADTIDKNHAIYEK - NS**K**NQGIEEALK | E554 | K219 |
| 20985 | 3469.67 | 3.01 | NYVTETNA**D**TIDKNHAIYEK - NLGPGMT**K**MAK | D558 | K170 |
| 22936 | 3468.66 | 2.62 | NYVT**E**TNADTIDKNHAIYEK - NLGPGMT**K**MAK | E554 | K170 |
| 23137 | 4011 | 3.29 | NYVTETNADTI**D**KNHAIYEK - VG**K**ETVQTTEDQILK | D561 | K59 |
| 25418 | 3725.82 | 3.27 | NYVTETNADTID**K**NHAIYEK - ETVQTT**E**DQILK | K562 | E66 |
| 25418 | 3725.82 | 3.72 | NYVTETNADTID**K**NHAIYEK - **E**TVQTTEDQILK | K562 | E60 |
| 27618 | 3161.66 | 3.21 | **G**SPGIPGDTYLTR - VGKETVQTT**E**DQILKR | G517 | E60 |
| 27618 | 3161.66 | 3.61 | **G**SPGIPGDTYLTR - VGKETVQTTE**D**QILKR | G517 | D67 |
| 28366 | 2918.61 | 3.18 | EVSSALS**K**VLSK - VGK**E**TVQTTEDQILK - | K579 | E66 |
| 29996 | 1977.96 | 3.06 | **G**SPGIPGDTYLTR - MI**D**ER | G517 | D176 |
| 36497 | 2772.45 | 3.78 | **G**SPGIPGDTYLTR - AQQVSQGL**D**VLTAK | G517 | D361 |
| 36615 | 4613.23 | 3.68 | IDDTSAELLT**D**DISDLKNNNDITAENNNIYK - NLGPGMT**K**MAK | D594 | K170 |
| 36632 | 2214.27 | 3.22 | A**K**EVSSALSK **-** **E**LLPVLISAMK - | K571 | E200 |
| 37536 | 3824.86 | 2.64 | **G**SPGIPGDTYLTR - KI**D**AAQNWLADPNGGPEGEEQIR | G517 | D389 |

| | | | | | |
|---|---|---|---|---|---|
| 40263 | 3413.78 | 3.79 | GSPGIPG**D**TYLTR - AQQVSQGLDVLTA**K**VENAAR | D484 | K366 |
| 40432 | 5992.94 | 5.1 | IDDTSA**E**LLTDDISDLKNNNDITAENNNIYK - GQGSSPVAMQKAQQVSQGLDVLTA**K** | E590 | K362 |
| 40679 | 2708.42 | 3.25 | S**K**DITK - GILSGTSDLLLTFD**E**AEVR | K526 | E128 |
| 40994 | 3074.69 | 3.12 | **K**VTNSLSNLISLIGTK - ETVQTTEDQILK | K498 | E66 |
| 41187 | 4612.22 | 2.86 | IDDTSA**E**LLTDDISDLKNNNDITAENNNIYK - NLGPGMT**K**MAK | E590 | K170 |
| 41816 | 2387.41 | 3.65 | DVTTSLS**K**VLK - **E**LLPVLISAMK | K625 | E200 |
| 43326 | 3137.65 | 3.41 | AAKDVTTSLS**K** - GILSGTSDLLLTFD**E**AEVR | K625 | E128 |
| 43537 | 3542.88 | 3.63 | IDDTSAELLT**D**DISDLK - ALA**K**QVATALQNLQTK | D594 | K464 |
| 43612 | 3604.91 | 3.34 | VTNSLSNLISLIGT**K**SGTQER - ETVQTT**E**DQILK | K513 | E66 |
| 45081 | 3350.71 | 3.48 | **G**SPGIPGDTYLTR - GILSGTS**D**LLLTFDEAEVR | G517 | D121 |
| 53474 | 5745.03 | 4.09 | NIN**K**D - TIESILEPVAQQISHLVIMHEEG**E**VDGKAIPDLTAPV AAVQAAVSNLVR | K632 | E31 |
| | | | | | |
| **#** | **Exp. MH$^+$** | **Primary Score** | **Peptide Sequence** | **Hv D1D2** | |
| 17582 | 1670.89 | 3.51 | VG**K**ETVQTT**E**DQILK | K59 | E66 |
| 17582 | 1670.89 | 3.38 | VG**K**ETVQTTE**D**QILK | K59 | D67 |
| 26000 | 3322.71 | 4.03 | LNQA**K**GWLRDPSASPGDAGEQAIR - ALASI**D**SK | K281 | D374 |
| 30901 | 3169.64 | 3.79 | GQGSSPVAMQ**K**AQQVSQGLDVLTAK - V**E**NAAR | K352 | E368 |
| 31031 | 3695.87 | 3.81 | LNQA**K**GWLRDPSASPGDAGEQAIR - MSA**E**INEIIR | K281 | E240 |
| 35827 | 3665.8 | 3.75 | **K**IDAAQNWLADPNGGPEGEEQIR - MSA**E**INEIIR | K387 | E240 |

| | | | | | |
|---|---|---|---|---|---|
| 38215 | 3040.71 | 3.43 | VG**K**ETVQTTEDQILKR - ELLPVLISAM**K** | K59 | K200 |
| 39734 | 3614.9 | 4.15 | GQGSSPVAMQ**K**AQQVSQGLDVLTAK - SLG**E**ISALTSK | K352 | E437 |
| 40218 | 3580.72 | 3.88 | VLQLTSWDEDAWAS**K**DTEAMK - MSA**E**INEIIR | K261 | E240 |
| 40418 | 2881.63 | 3.77 | QVATALQNLQT**K**TNR - ELLPVLISAM**K** | K476 | E200 |
| 40559 | 3184.71 | 4.71 | AQQVSQGLDVLTA**K**VENAAR - SLG**E**ISALTSK | K366 | E437 |
| 40560 | 2280.32 | 3.35 | ELLPVLISAM**K** - LNQA**K**GWLR | E200 | K281 |
| 40604 | 2553.46 | 3.78 | ALASIDS**K**LNQAK - ELLPVLISAM**K** | K276 | E200 |
| 41140 | 2892.69 | 3.97 | ALA**K**QVATALQNLQTK - ELLPVLISAM**K** | K464 | E200 |
| 41598 | 4173.16 | 5.49 | GQGSSPVAMQKAQQVSQGLDVLTA**K**VENAAR - KL**E**AMTNSK | K366 | E375 |
| 41598 | 4173.16 | 5.8 | GQGSSPVAMQKAQQVSQGLDVLTA**K**VENAAR - **K**LEAMTNSK | E368 | K373 |
| 41598 | 4173.16 | 4.98 | GQGSSPVAMQKAQQVSQGL**D**VLTAK - VENAAR**K**LEAMTNSK | D361 | K373 |
| 41682 | 3726.02 | 3.87 | GQGSSPVAMQ**K**AQQVSQGLDVLTAK - ELLPVLISAM**K** | K352 | E200 |
| 42387 | 3293.83 | 4.63 | AQQVSQGLDVLTA**K**VENAAR - ELLPVLISAM**K** | K366 | E200 |
| 42387 | 3293.83 | 3.3 | AQQVSQGLDVLTAKV**E**NAARK - LNQA**K**GWLR | E368 | K281 |
| | | | | | |
| **#** | **Exp. $MH^+$** | **Primary Score** | **Peptide Sequence** | **A483** | |
| 17398 | 3339.66 | 3.31 | NYVTETNADTI**D**KNHAIYEK - A**K**EVSSALSK | D561 | K571 |
| 17630 | 3341.68 | 3.44 | NYVTETNA**D**TIDKNHAIYEK - A**K**EVSSALSK | D558 | K571 |
| 17630 | 3341.68 | 4.19 | NYVT**E**TNADTIDKNHAIYEK - A**K**EVSSALSK | E554 | K571 |

| | | | | | |
|---|---|---|---|---|---|
| 20071 | 3141.53 | 3.53 | NYVTETNADTID**K**NHAIYEK - AK**E**VSSALSK | K562 | E572 |
| 20150 | 3349.69 | 4.44 | NYVTETNA**D**TIDKNHAIYEK - L**K**VTDANIR | D558 | K542 |
| 20150 | 3349.69 | 4.03 | NYVTETNADTI**D**KNHAIYEK - L**K**VTDANIR | D561 | K542 |
| 35163 | 4584.24 | 3.59 | IDDTSAELLT**D**DISDLKNNNDITAENNNIYK - AA**K**DVTTSLSK | D594 | K617 |
| 35163 | 4584.24 | 3.49 | IDDTSAELLTD**D**ISDLKNNNDITAENNNIYK - AA**K**DVTTSLSK | D595 | K617 |
| 35382 | 4586.24 | 3.35 | IDDTSA**E**LLTDDISDLKNNNDITAENNNIYK - AA**K**DVTTSLSK | E590 | K617 |
| 35967 | 4584.24 | 4.42 | IDDTSAELLTDDIS**D**LKNNNDITAENNNIYK - AA**K**DVTTSLSK | D598 | K617 |
| 35967 | 4584.24 | 4.95 | IDDTSAELLTDDISDLKNNNDITA**E**NNNIYK - AA**K**DVTTSLSK | E608 | K617 |
| 35967 | 4584.24 | 4.52 | IDDTSAELLTDDISDL**K**NNNDITAENNNIYK - AAK**D**VTTSLSK | K600 | D618 |
| 35967 | 4584.24 | 4.22 | IDDTSAELLTDDISDLKNNNDITAENNNIY**K** - AAK**D**VTTSLSK | K614 | D618 |
| 35967 | 4584.24 | 4.94 | IDDTSAELLTDDISDLKNNN**D**ITAENNNIYK - AA**K**DVTTSLSK | D604 | K617 |
| 39881 | 2845.52 | 4.73 | VTNSLSNLISLIGT**K**SGTQER - **E**LQEK | K513 | E520 |
| 39881 | 2845.52 | 4.62 | VTNSLSNLISLIGT**K**SGTQER - ELQ**E**K | K513 | E523 |
| 40044 | 4655.33 | 5.07 | IDDTSAELLT**D**DISDLKNNNDITAENNNIYK - DVTTSLSKVL**K** | D594 | K625 |
| 40044 | 4655.33 | 4.86 | IDDTSAELLTD**D**ISDLKNNNDITAENNNIYK - DVTTSLSKVL**K** | D595 | K625 |

| | | | | | |
|---|---|---|---|---|---|
| 40044 | 4655.33 | 4.45 | IDDTSAELLTDDIS**D**LKNNNDITAENNNIYK - DVTTSLSKVL**K** | D598 | K625 |
| 40044 | 4655.33 | 4.44 | IDDTSA**E**LLTDDISDLKNNNDITAENNNIYK - DVTTSLSKVL**K** | E590 | K625 |
| 40065 | 3092.6 | 3.51 | IDDTSAELLT**D**DISDLK - EVSSALSKVLS**K** | D594 | K579 |
| 40065 | 3092.6 | 3.38 | IDDTSAELLTD**D**ISDLK - EVSSALSKVLS**K** | D594 | K579 |
| 40069 | 3093.61 | 3.36 | IDDTSAELLTDDIS**D**LK - EVSSALSKVLS**K** | D598 | K579 |
| 40095 | 2988.61 | 4.48 | VTNSLSNLISLIGT**K**SGTQER - VT**D**ANIR | K513 | D545 |
| 40448 | 3252.74 | 3.81 | VTNSLSNLISLIGT**K**SGTQER - ETIF**E**ASKK | K513 | E494 |
| 40603 | 5153.62 | 4.36 | IDDTSAELLT**D**DISDLKNNNDITAENNNIYK - **K**VTNSLSNLISLIGTK | D594 | K498 |
| 40603 | 5153.62 | 4.46 | IDDTSAELLTD**D**ISDLKNNNDITAENNNIYK - **K**VTNSLSNLISLIGTK | D595 | K498 |
| 40603 | 5153.62 | 4.56 | IDDTSAELLTDDIS**D**LKNNNDITAENNNIYK - **K**VTNSLSNLISLIGTK | D598 | K498 |
| 40603 | 5153.62 | 3.99 | IDDTSAELLTDDISDLKNNN**D**ITAENNNIYK - **K**VTNSLSNLISLIGTK | D604 | K498 |
| 40606 | 5153.62 | 3.53 | IDDTSA**E**LLTDDISDLKNNNDITAENNNIYK - **K**VTNSLSNLISLIGTK | E590 | K498 |
| 41116 | 2593.44 | 3.85 | **K**VTNSLSNLISLIGTK - **E**TIFEASK | K498 | E490 |
| 41142 | 3909.09 | 4 | **E**TIFEASKKVTNSLSNLISLIGTK - **G**SPGIPGDTYLTR | E490 | G477 |

**Suppl. Table 3**. Cross-linked residues characterized in the D1D2 -A483 1:1 complex (XL-amino acids of each protein are bolded in the sequences)

642

643

644 **Suppl. movie 1.** TIRF analysis of HV-mCherry expressing C2.7 cells co-transfected with a GFP fusion to
645 the indicated construct. The time is indicated in seconds.

646

647 **Suppl. movie 2.** TIRF analysis of HV-mCherry expressing C2.7 cells co-transfected with a GFP fusion to
648 the indicated construct. The time is indicated in seconds. At time "0", addition of the Rho kinase inhibitor
649 Y-27632 was added at 100 µM final concentration.

650

651 **Suppl. movie3.** TIRF analysis of VASP-mCherry expressing C2.7 cells co-transfected with a GFP fusion to
652 the indicated construct. The time is indicated in seconds. At time "0", addition of the Rho kinase inhibitor
653 Y-27632 was added at 100 µM final concentration.

654

655 **Suppl. Movie 4.** 1205Lu melanoma cells 1205Lu melanoma cells were transfected with the indicated
656 constructs. Cells were perfused in a microfluidic chamber and allowed to adhere for 20 min prior to
657 application of shear stress reaching 22.2 dynes.cm$^{-2}$. The elapsed time is indicated in seconds.